Studies on Organic Magnetic Resonance Contrast Agents for Medical Imaging

Maiju Soikkeli

Department of Chemistry
Faculty of Science
University of Helsinki
Finland

Academic Dissertation

To be presented, with the permission of the Faculty of Science, University of Helsinki, for public examination in Auditorium E204, Department of Physics, Gustaf Hällströmin katu 2, on November 29th, at 12 noon.

Helsinki 2019

Supervisor

Docent Sami Heikkinen
Department of Chemistry
University of Helsinki
Finland

Reviewers

Professor Olli Gröhn
A. I. Virtanen Institute for Molecular Sciences
University of Eastern Finland
Finland

Professor Pasi Virta
Department of Chemistry
University of Turku
Finland

Opponent

Docent Elina Sievänen
Department of Chemistry
University of Jyväskylä
Finland

ISBN 978-951-51-5591-7 (paperback)
ISBN 978-951-51-5592-4 (PDF)
http://ethesis.helsinki.fi

Unigrafia
Helsinki 2019

"A jack of all trades is a master of none,
but oftentimes better than a master of one."

— Anonymous

Abstract

Magnetic resonance imaging (MRI) is one of the most important medical imaging methods due to its noninvasiveness, superior versatility and resolution. In order to improve the image quality and to make different tissues more distinguishable, MRI is often used together with contrast agents. Contrast agents are most commonly based on gadolinium. However, during recent decades, the group of metal-free contrast agents has become a major area of development. One striking group of potential metal-free contrast agents are the nitroxides, stable organic radicals.

In this thesis, two fully organic, metal-free nitroxides were designed and synthesized. The compounds consisted of a nitroxide moiety bearing the contrast enhancing properties and a targeting moiety aimed to invoke specificity of the agent towards tumor tissue. Their stability and relaxation enhancing properties were determined in order to evaluate their potential as novel contrast agents for MRI. Both of the compounds proved to be highly stable by maintaining their contrast and relaxation enhancing properties for several hours is harsh conditions. Also, they displayed effective relaxation time shortening in MRI experiments. Therefore, these organic radical contrast agents are expected to bring a noteworthy addition to the established MRI-based diagnostics by joining the growing group of metal-free contrast agents for MRI.

Another medical diagnostic method based on magnetic resonance is magnetic resonance spectroscopy (MRS) and spectroscopic imaging (MRSI). In the latter section of the thesis a novel organic marker for MRS and MRSI with no existing equivalent was developed. Although the phantom MRS studies seemed promising, unfortunately the *in vivo* animal studies did not give the desired outcome leaving place for improvement.

List of Publications

The thesis is based on the following publications:

I. **M. Soikkeli**, K. Sievänen, J. Peltonen, T. Kaasalainen, M. Timonen, P. Heinonen, S. Rönkkö, V.-P. Lehto, J. Kavakka and S. Heikkinen. Synthesis and *in vitro* phantom NMR and MRI studies of fully organic free radicals, TEEPO-glucose and TEMPO-glucose, potential contrast agents for MRI. *RSC Adv.* **2015**, *5*, 15507 - 15510.

II. **M. Soikkeli**, K. Horkka, J.O. Moilanen, M. Timonen, J. Kavakka and S. Heikkinen. Synthesis, Stability and Relaxivity of TEEPO-Met: An Organic Radical as a Potential Tumor Targeting Contrast Agent for Magnetic Resonance Imaging. *Molecules* **2018**, *23*, 1034.

III. **M. Soikkeli**, M.I. Kettunen, R. Nivajärvi, V. Olsson, S. Rönkkö, J.P. Laakkonen, V.-P. Lehto, J. Kavakka and S. Heikkinen. Assessment of the Relaxation Enhancing Properties of a Nitroxide-Based Contrast Agent TEEPO-Glc with *in vivo* Magnetic Resonance Imaging. *Submitted*

The publications are referred to in the text by their roman numerals.

Author contributions

The contributions of the authors in articles I–III can be separated as follows:

I. The author performed the synthesis of TEEPO-Glc, measured the *in vitro* NMR experiments together with KS under the supervision of JK and SH. The author analyzed *in vitro* NMR and MRI data under supervision of SH. KS performed the synthesis of TEMPO-Glc. JP, TK and MT performed the MR imaging. PH performed the MS analysis of the compounds. SR performed the cell viability study under supervision of VPL. All authors contributed in writing the manuscript.

II. The author performed the synthesis of the contrast agent, the *in vitro* NMR study and as well as the analysis of the MRI study under the supervision of SH. KH performed the synthesis of the precursor 4-hydroxy-TEEPO. JOM performed the EPR measurements and analyzed the results. MT performed the MR imaging. The author drafted the manuscript with assistance of all authors.

III. The author prepared the contrast agent and designed the *in vivo* MRI study together with MIK and SH. RN and VO were responsible for the tumor model. MIK performed the MR imaging and anazysed the results. SR, JPL and VPL conducted the *in vitro* cytotoxicity studies. SH and JK were behind the initial idea. The author prepared the manuscript with contribution of all authors.

Preface

This work was carried out in the Department of Chemistry, University of Helsinki during years 2014–2019 under supervision of docent Sami Heikkinen. Funding from the University of Helsinki Research Foundation, the doctoral programme in Chemistry and Molecular Sciences (CHEMS), Finnish Cultural Foundation and Alfred Kordelin Foundation (Gust. Komppa fund) are gratefully acknowledged.

First of all I want to thank my supervisor Sami Heikkinen. I started to work in this project already during my MSc studies. As enjoyable as working on my master's thesis was, little did I know what a roller-coaster doing a PhD would be. Thank you for helping me through it all and always having time for me and my questions. Also, thanks for the hilarious trips we have had together.

I am grateful to Prof. Ilkka Kilpeläinen for your support through all my studies from an undergraduate to a PhD student. I also want to thank you for providing me with excellent research facilities and an inspiring environment.

This thesis was reviewed by Prof. Olli Gröhn and Prof. Pasi Virta. With your careful reviews and valuable comments I was able to make this thesis better. Also docent Elina Sievänen is appreciated for kindly agreeing to be my opponent.

I want to thank Dr. Jari Kavakka, my MSc supervisor, who convinced me to pursue (or fooled me into pursuing) my studies and choose to become a PhD student. Thank you for all your advice and inspiration.

This work would not have been possible without the contribution of my excellent collaborators. Dr. Marjut Timonen, Dr. Touko Kaasalainen and Dr. Juho Peltonen from the HUS Medical Imaging Center, thank you for teaching me MRI and welcoming me to the clinical scanners. Dr. Mikko Kettunen and his colleagues in the A.I. Virtanen Institute for Molecular Sciences are greatly acknowledged for their efforts in the *in vivo* MRI studies. I also want to acknowledge Prof. Vesa-Pekka Lehto, Dr. Seppo Rönkkö and Dr. Johanna Laakkonen from the University of Eastern Finland for providing the cytotoxicity assays. I am deeply grateful to Dr. Jani Moilanen from University of Jyväskylä not only for his valuable help with EPR but also our scientific discussions both on and off duty. I also want to thank Dr. Petri Heinonen for

helping me with MS spectroscopy.

A special thanks goes to my best lab-buddies Katja Sievänen and Kaisa Horkka, not only for your excellent work in the lab but also for all the good times outside the lab. I was lucky to be able to work with someone who I could also call my friends.

I am especially grateful to my peers, Dr. Tia Kakko, Hanna Niemikoski and Sofia Otaru, with whom I have shared all the ups and downs during the last stages of this process. Your support has been irreplaceable. Also, the personnel from the Department of Chemistry and the former laboratory of organic chemistry are greatly acknowledged.

This work would not have been possible without the support and encouragement from my friends and family. I would like to thank my best friends Mervi, Minna, Päivi and Sanna for all our adventures and most importantly giving me other things to think about. A special thanks goes to my two very dear furry friends Kielo and Rauli. Kielo, thank you for forcing me out of my chamber for our daily walks. Rauli, thank you for not deleting my thesis while sitting on my laptop. I want to thank my dear family, my parents, Tuula and Pertti, my mother-in-law Kirsi, and my brother Jyrki and his wife Heidi. Kiitos äiti ja isä kaikesta rakkaudesta ja tuesta, jota olen vuosien varrella teiltä saanut.

The biggest thanks belongs to my husband Sampsa. Without you, this process would have been if not impossible, at least a lot more difficult. You have been my proofreader, personal IT support and general advisor. Most importantly, you have been an understanding and loving companion, thank you for everything.

Helsinki, October 2019
Maiju Soikkeli

Contents

List of Abbreviations

B_0	External magnetic field
B_1	Magnetic field produced by the radio frequency pulse
γ	Gyromagnetic ratio
I	Spin quantum number
^2J	Geminal coupling constant
^3J	Vicinal coupling constant
M	Net magnetization
μ	Magnetic moment
ω_0	Larmor frequency
q	Hydration number
R_1, R_2	Longitudinal and transverse relaxation rate
r_1, r_2	Longitudinal and transverse relaxivity
T_1, T_2	Longitudinal and transverse relaxation time
τ_R	Rotational correlation time
τ_M	Water residence lifetime
θ	Flip angle
AgOTf	Silver trifluoromethanesulfonate
ATP	Adenosine triphosphate
BASP	Brush-arm star polymer
BBB	Blood–brain barrier
Boc	*tert*-butyloxycarbonyl
CEST	Chemical exchange saturation transfer
CHESS	CHEmical Shift-Selective
Cho	Choline containing compounds
CLIO	Cross-linked iron-oxide
CSF	Cerebrospinal fluid
CSI	Chemical shift imaging
CT	Computed tomography
DAB	Polypropyleneimine dendrimer
DCC	*N,N'*-Dicyclohexylcarbodiimide
DCM	Dichloromethane

DESPOT	Driven Equilibrium Single Pulse Observation of T_1
DHA—AA	Dehydroascorbic acid—ascorbic acid
DIACEST	Diamagnetic chemical exchange saturation transfer
DMAP	4-Dimethylaminopyridine
DME	1,2-Dimethoxyethane
DNP	Dynamic nuclear polarization
EMA	European Medicines Agency
endo-CEST	Endogenous chemical exchange saturation transfer
EPR(I)	Electron paramagnetic resonance (imaging)
ESI	Electron spray ionization
FDA	U.S Food and Drug Administration
FID	Free induction decay
FLASH	Fast low angle shot
FOV	Field of view
DAB	Polypropyleneimine
GBCA	Gadolinium-based contrast agent
Gd(BOPTA)	Gadobenic acid
Gd(DO3A-butrol)	Gadobutrol
Gd(DOTA)	Gadoteric acid
Gd(DTPA)	Gadopentetate dimeglumine
Gd(DTPA-BMA)	Gadodiamide
Gd(DTPA-BMEA)	Gadoversetamide
Glc	Glucose
Gln	Glutamine
Glu	Glutamate
H-Met-OMe · HCl	L-Methionine methyl ester hydrochloride
HeLa	Henrietta Lacks cell line
HMBC	Heteronuclear Multiple Bond Correlation
HOBt	1-Hydroxybenzotriazole
HP	Hyperpolarized / Hyperpolarization
HUVEC	Human umbilical vein endothelial cells
Lac	Lactate
LDH	Lactate dehydrogenase
LUMO	Lowest unoccupied molecular orbital
ME	Metastability exchange
Met	Methionine
mI	Myo-inositol
MION	Monocrystalline iron-oxide
MRI	Magnetic resonance imaging
MRS	Magnetic resonance spectroscopy

MRSI	Magnetic resonance spectroscopic imaging
MS	Mass spectroscopy
NAA	*N*-Acetyl aspartate
NMM	4-Methylmorpholine
NMR	Nuclear magnetic resonance
NSF	Nephrogenic systemic fibrosis
PAMAM	Polyamidoamine dendrimer
PBS	Phosphate buffered saline
PD	Proton density
PEG	Poly(ethylene glycol)
PET	Positron emission tomography
PHIP	Parahydrogen-induced polarization
PRESS	Point resolved spectroscopy
RF	Radio frequency
ROI	Region of interest
RT	Room temperature
SABRE	Signal amplification by reversible exchange
SD	Standard deviation
SEOP	Spin-exchange optical pumping
SNR	Signal-to-noise ratio
SOMO	Singly occupied molecular orbital
SPIO	Superparamagnetic iron-oxide
STEAM	Stimulated Echo Acquisition Mode
SVS	Single voxel spectroscopy
SW	Spectral width
tCr	Total creatine
TE	Echo time
TEEPO	2,2,6,6-Tetraethylpiperidin-1-oxyl
TEMPO	2,2,6,6-Tetramethylpiperidin-1-oxyl
TFA	Trifluoroacetic acid
THF	Tetrahydrofuran
TMS	Trimethylsilyl
TMSEt-Glc	(2-(Trimethylsilyl)ethyl β-D-glucopyranoside)
TOSMIC	*p*-Toluenesulfonyl methyl isocyanide
TR	Repetition time
USPIO	Ultrasmall superparamagnetic iron-oxide
VAPOR	VAriable Power pulses with Optimized Relaxation delays
VOI	Volume of interest
WET	Water suppression Enhanced Through T_1
Å	Ångström

1 Introduction

1.1 Magnetic resonance imaging

Nuclear magnetic resonance (NMR) phenomenon has become an important tool for chemists, physicist as well as medical professionals. The first experiments to detect and measure the magnetic properties of atoms and molecules are dating back the 1940s.[1–3] Since those times, NMR spectroscopy has become commonplace as a structural characterization method in many research laboratories. In the 1970s, the NMR phenomenon was refined to study subjects *in vivo* by introducing gradients to the magnetic field.[4–7] The method featured localization of the signals to produce images with spatial information and to create anatomical images. The method was called magnetic resonance imaging (MRI), and the first scanners appeared in clinical use in the 1980s.

MRI is a versatile imaging method that can be used in neuro-, cardiovascular and musculoskeletal imaging as well as in angiography. The imaging is based on creating contrast between different tissue types or malignant and healthy tissue. The contrast can be further improved with optimization of imaging parameters and pulse sequences, or utilizing contrast agents. This thesis will focus on contrast enhancement with contrast agents. Constant progress for developing more efficient scanners, superior resolution and non-invasiveness have made MRI one of the most important diagnostic media. Also, currently the moderate expenses have made MRI instruments readily available in majority of hospitals.

1.1.1 Basic principle of MRI

The main difference between MRI and for example X-ray or computer tomography (CT) is the utilization of magnetic fields and radio frequency (RF) pulses rather than ionizing radiation. Also, it does not apply radioactive tracers like positron emission tomography (PET). MRI typically measures the magnetic properties of the hydrogen nuclei of water molecules, the most abundant species in living organisms. Hydrogen nuclei, or protons, are spinning charged particles with a spin quantum number (I) of $1/2$, that produces a local magnetic field

called magnetic moment. Upon application of an external magnetic field, the spins start to precess at Larmor frequency (ω_0) (Figure 1.1). The Larmor frequency is proportional to the strength of the magnetic field and gyromagnetic ratio (γ) that is specific for each nucleus. For hydrogen, the gyromagnetic ratio is 42.58 MHz/T meaning that the magnetic moment μ of ^{1}H nuclei precesses at 42.58 MHz frequency in a 1.0 T magnetic field.

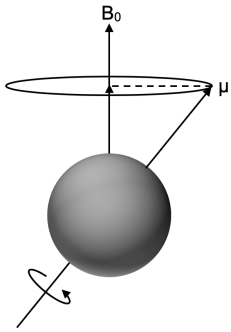

Figure 1.1 Precession of a nuclear spin in an external magnetic field.[8]

The application of the external magnetic field B_0, also generates a net magnetization (M) along the field as the majority of the spins align themselves parallel to the magnetic field. The phenomenon is commonly described by a vector model, where B_0 and M are considered to be placed along the z-axis. Measuring the small net magnetization parallel to an extremely powerful B_0 is virtually impossible. Therefore, the alignment of the net magnetization is manipulated by an RF pulse oscillating at Larmor frequency. A pulse given at the Larmor frequency utilizes resonance effect and is powerful enough to distort the net magnetization away from the strong B_0. This generates a magnetic field B_1 on the transverse plane.

Upon the application of the RF pulse, the net magnetization begins to precess about the B_1 and the M rotates away from the z-axis (Figure 1.2a). Due to the simultaneous precession about the z-axis, the rotation occurs as a spiral motion. Therefore, in order to simplify the vector model, it is commonly presented in a rotating frame where B_1 is set parallel to x'-axis. As in Figure 1.2a, a 90° RF pulse flips the magnetization into the transverse plane (Figure 1.2b). After the RF pulse is switched off, the precession occurs solely along the z-axis. The receiver coil set on the transverse plane detects this as an oscillating magnetic field. Simultaneously, the net magnetization starts to return to the thermal equilibrium state by realigning itself along the z-axis. Also, the individual spins precessing together begin to dephase and lose co-

herence. As a result of these processes, longitudinal and transverse relaxation, respectively, the detected signal starts to decay over time, which is collected by the detector as a free induction decay (FID) (Figure 1.2c).

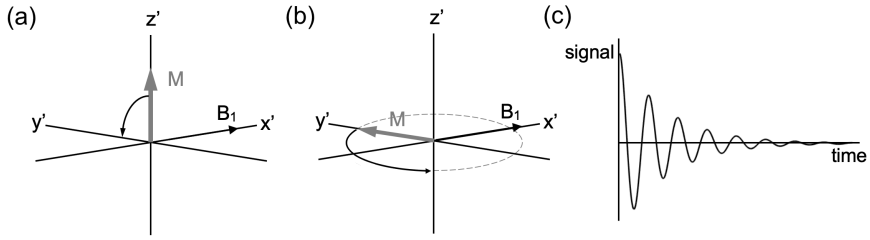

Figure 1.2 A simple vector model on the effect of RF radiation. (a) The net magnetization M begins to precess about the magnetic field B_1. (b) After a 90° RF pulse, the net magnetization M is in the transverse plane. The flipped magnetization starts to precess along the z-axis. (c) The signal is collected at the receiver coil as a free induction decay (FID).

1.1.2 Relaxation

The image contrast is built on various factors. These include proton density, different imaging parameters and most importantly the relaxation of protons. The foundations for the NMR relaxation theory were laid in the 1940s by Bloembergen Purcell and Pound.[9] The relaxation phenomenon is a complex process involving various factors making its detailed description laborious.[10–12] Furthermore, in living tissue, a large variety of molecular environments further complicates the process.[8] In brief, relaxation in MRI is mainly based on dipole-dipole interactions. These interactions take place between nuclei that are in constant motion, which generates fluctuating magnetic fields with a broad frequency band.[13] The dipole-dipole interactions between nuclei and unpaired electrons are remarkably stronger than between nuclei due to the large magnetic moment of the electron. Contrast agents as relaxation enhancing substances are based on this effect, and they will be discussed in more detail in section 1.1.3.

As described in the previous section, there are two types of relaxations following the RF pulse; longitudinal and transverse relaxation. Transverse relaxation (T_2), or spin-spin relaxation, is the process where excited spins lose their phase coherence.[14] This is due to small inconsistencies in the magnetic field contributed by each spin locally, which changes the precession frequencies of the neighboring spins. As the spins adapt their precession frequency

to the fluctuating magnetic field, they eventually become totally out of phase in regard to each other. Longitudinal relaxation (T_1) is where the net magnetization realigns itself along the z-axis as spins give up the energy obtained from the RF pulse to the surrounding lattice. Therefore, it is also known as spin-lattice relaxation.

As relaxation is closely linked to the motion of the nuclei, it is convenient to introduce a time constant called rotational correlation time (τ_R). It describes roughly the time between two successive reorientations of the molecule.[13] Taking account the resonance effect, the most effective T_1 relaxation is obtained when $\omega_0\tau_R \approx 1$.[15] Thus, the T_1 of medium-sized molecules is short, while small molecules with short rotational correlation times have long T_1, as well as large molecules with long τ_R. In turn, T_2 relaxation is most effective, when τ_R is long. Therefore, the T_2 shortens as the molecular size increases.

The water molecules in living tissue can roughly be divided into three groups: bound-, structured- and free water.[14] Free water, for example cerebrospinal fluid (CSF), moves around rapidly and has small τ_R. Due to its constant change in motion, tumbling occurs over a wide range of frequencies. Therefore, only small amount of fluctuations take place at Larmor frequency resulting in long T_1 (Figure 1.3). Also, the fast fluctuation causes rapid changes in the local magnetic field and the field relative to proton seems homogenous. This phenomenon, often referred to as motional averaging, causes slow dephasing and long T_2. Correspondingly, water bound to large macromolecules has long τ_R leading to long T_1 but short T_2. Most of the water in tissues is so called structured water that is somewhere between the free and bound water. It tumbles at a frequency quite near the Larmor frequency generating short T_1 and medium T_2.

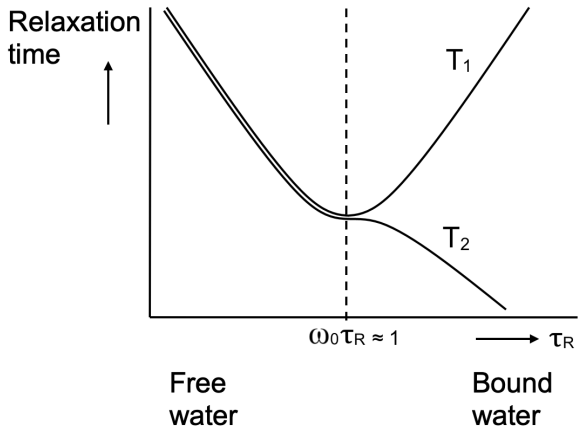

Figure 1.3 The effect of rotational correlation time τ_R on relaxation times T_1 and T_2. Adapted from Bloembergen et al.[9]

In MRI, the contrast corresponds to differences in signal intensities describing divergent tissues, that make the image more distinguishable. The contrast can be controlled by varying the imaging methods and using different weightings. For instance, choosing the sequence parameters so that the contrast reflects mainly the variations in T_1 corresponds to T_1-weighting. Echo time and repetition time are critical parameters in creating different weightings. Echo time (TE) is the time from the center of the RF pulse to the center of the echo (the peak of the time domain signal) whereas repetition time (TR) is the time between successive RF pulses.

As the recovery of the magnetization along the z-axis is due to the longitudinal relaxation T_1, it can be emphasized by optimizing the TR. Increasing TR long enough eventually enables complete T_1 relaxation. This creates high signal intensities for all tissue types, but simultaneously the contrast between tissue types decreases as the signal intensities become closer to each other. If TR is short, the longitudinal magnetization will be partially saturated leading to lower signal intensity. The degree of saturation and thus the signal intensity depend on tissue T_1 leading to contrast between tissues with different T_1 values. During TE, the transverse magnetization decreases due to T_2 relaxation. Thus, as TE increases, the signal intensity decreases. However, the effect of TE on the intensities and contrast depends on the T_2 value of the tissue under study. With these facts in mind, for T_1-weighting TE and TR should be short for maximized T_1- and minimized T_2 contrast. Similarly, T_2-weighting is obtained by selecting long TE and TR. Tissues with short T_2 appear as darkened areas in T_2 weighted images whereas tissues with short T_2 will appear bright in T_1-weighted images. Minimizing both T_2 and T_2 contrasts by selecting short

TE and long TR, creates a proton density (PD) image. In PD scans, the brightness of the image is determined by the number of protons in the area of interest.

1.1.3 Contrast agents

In general, substantial part of MRI development focuses on imaging techniques but also the significance of contrast agents has grown over time. There are countless ways to categorize contrast agents but probably the most favored one is to highlight two main groups, T_1 and T_2 contrast agents. The majority of contrast agents are based on paramagnetic metals. They possess unpaired electrons that induce a positive magnetic susceptibility and can alter the surrounding magnetic field.[16] Due to the local changes in the magnetic field and the dipolar interactions between protons and unpaired electrons, paramagnetic agents act as relaxation enhancers. This causes shortening in the relaxation times of the protons in the near vicinity. The relaxation enhancing efficiency is often described with the term relaxivity. Relaxivities r_1 and r_2 are measures of a change in the relaxation rates R_1 and R_2 ($1/T_1$ and $1/T_2$, respectively) normalized to the contrast agent concentration. Usually, they are defined by the slopes of R_1 and R_2 as a function of concentration.

In addition to the contrast agent concentration, other important factors in relaxation enhancement are related to the structures of the contrast agents.[17] Hydration number (q) indicates the amount of water molecules that can coordinate to the contrast agent molecule at a time. The larger the number, the better the efficiency of the contrast agent is. In addition, the distance between the water molecule and the paramagnetic center correlates with the relaxation efficiency. The relaxation is most effective when the distance is short. Of the dynamic factors, rotational correlation time (τ_R), and water residence lifetime (τ_M) are the most relevant ones. As presented earlier, rotational correlation time describes the movement of the molecule. Contrast agents with long τ_R have generally better relaxivity. The residence lifetime of the bound water is the time water molecules stay in contact with the contrast agent molecule. The residence time should be long enough for the water molecules to become fully relaxed, but short enough to optimize the water exchange rate, leading to the most efficient relaxation.[18]

1.1.3.1 T_1 contrast agents

T_1 contrast agents are known to shorten escpecially the T_1 time of the nearby nuclei. This is observed as a brightening of the image in T_1-weighted MRI. The clear majority of clinically used contrast agents is based on the paramagnetic

metal gadolinium (Gd^{3+}).[19–21] Also, the first contrast agent approved for clinical use was gadolinium-based. This agent was Gd(DTPA) (gadopentetate dimeglumine) (**1**, Scheme 1.1) also known as Magnevist by Schering AG.[22–27] The popularity of gadolinium-based contrast agents (GBCAs) can be credited mainly to three unique characteristics of gadolinium; the large number of unpaired electrons, high magnetic moment and long electron spin relaxation. Gadolinium has seven unpaired electrons inducing a powerful magnetic moment. The symmetry of the electronic state of gadolinium elongates the electron spin relaxation outclassing some other lanthanides with stronger magnetic moments.

In human body, free gadolinium is higly toxic. As the ionic radius of Gd^{3+} is close to Ca^{2+}, it can bind to Ca^{2+} ion channels and replace calcium in Ca^{2+} binding enzymes and proteins.[21,28] In order to reduce the toxicity, the metal ions are bound to ligands. However, in some cases the chelation may have a negative effect on the relaxation enhancing properties. The contrast agents are required to be thermodynamically stable and kinetically inert. Usually, the kinetic properties are more substantial than thermodynamic properties as the time the agents spend in human body before excretion through kidneys is small (biological half-life 1.5 h). Table 1.1 lists the six most common GBCAs, including their generic and trade names, as well as their r_1 values measured in 1.5 T and 3.0 T fields.[29] The molecular structures are given in Scheme 1.1.

Table 1.1 Common Gd-based MRI-contrast agents.

Chemical name	**Generic name**	**Trade name**	r_1*	
			1.5 T	**3 T**
Gd(DTPA) (**1**)	Gadopentetate dimeglumine	Magnevist	4.1	3.7
Gd(DTPA-BMA) (**2**)	Gadodiamide	Omniscan	4.3	4.0
Gd(DTPA-BMEA) (**3**)	Gadoversetamide	OptiMARK	4.7	4.5
Gd(BOPTA) (**4**)	Gadobenic acid	MultiHance	6.3	5.5
Gd(DOTA) (**5**)	Gadoteric acid	Dotarem	3.6	3.5
Gd(DO3A-butrol) (**6**)	Gadobutrol	Gadovist	5.2	5.0

*in plasma at 37 °C (mM^{-1} s^{-1})

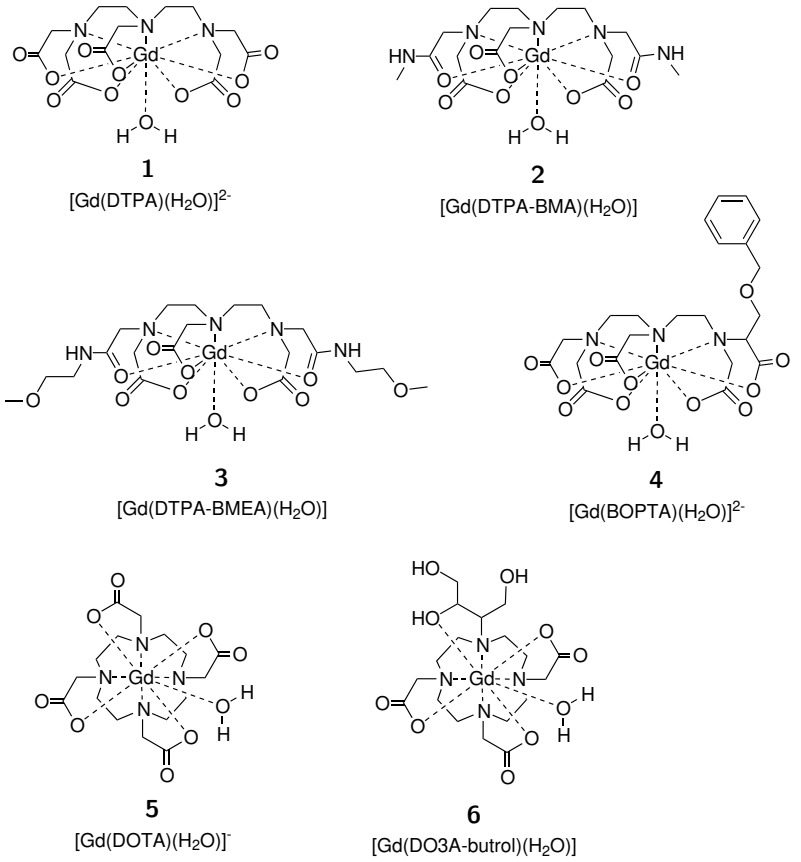

Scheme 1.1 Structures of common Gd-based MRI-contrast agents.

Compounds (**1**–**4**) have linear structures whereas (**5**–**6**) are macrocycles. It has been noted that cyclic GBCAs are more inert than the linear agents. The ionic charge affects the stability, ionic agents (**1**, **4**, and **5**) being more stable than the non-ionic ones. The possible mechanisms for the Gd^{3+} release from the contrast agents are transmetallation, transchelation and metal dissociation.[20] Gadolinium-based contrast agents were considered fully safe until 2006, when it was first reported, that they may cause a condition called nephrogenic systemic fibrosis (NSF).[30] Patients with renal disorders should not be subjected to GBCA injections during imaging. The disease causes fibrosis of sceletal muscle and visceral organs with no effective treatment.[31–33]

A study by Kanda et al.[34] revealed Gd accumulating in brain even for patients with no renal dysfuction. Typically the deposition is observed with patients subjected to repeated GBCA administrations.[35–37] For the these reasons, FDA (Food and Drug Administration) gave new recommendations to avoid repeated use of GBCAs[38] and EMA (European Medicines Agency) a re-

ferral to suspend or restrict use of the four linear GBCAs (**1**–**4**, Scheme 1.1).[39] Furthermore, anthropogenic gadolinium has been found in aquatic environment migrated through waste-water.[40,41] Traces of gadolinium have even been found from drinking water.[42] For these reasons, the research community has initiated to seek new groups of contrast agents.

In addition to gadolinium-based contrast agents, there are examples of T_1 contrast agents based on manganese.[43,44] However, they have not progressed to clinical use.

1.1.3.2 T_2 contrast agents

All MRI contrast agents shorten both T_1 and T_2 relaxation times. However, while gadolinium increases somewhat similar amounts of R_1 and R_2, in tissue the relative change in R_1 is much larger than in R_2.[19] The r_1 often also experiences slight decrease in stronger magnetic fields, whereas r_2 is not affected. T_2 contrast agents are mainly superparamagnetic iron nanoparticles due to their anisotropic susceptibility effects. The use of nanoparticles enables functionalization for selective targeting, multimodality, and therapy applications. The oxide is often coated with dextran, carboxydextran or silicates. Currently, there are superparamagnetic iron oxide 50-500 nm (SPIO), ultrasmall superparamagnetic 4-50 nm (USPIO), monocrystalline (MION) and cross-linked (CLIO) contrast agents.[45] These are specifically used in liver imaging.[46] However, due to severe allergic reactions caused by many SPIO agents, their development has been stopped and some have even been withdrawn from the market.[47]

1.1.3.3 Metal-free contrast agents

As an alternative to metal-based contrast agents, some metal-free contrast enhancement methods for MRI have been developed. Probably the two most important ones are chemical exchange saturation transfer (CEST) and hyperpolarized (HP) techniques. The first method, CEST is a technique which probes saturation of exchangeable protons in the target molecules.[48] Exchangeable protons can be found for example in agents containing amine (-NH_2) and carboxylic (-COOH) groups. The contrast in CEST is based on the decrease in the bulk water signal intensity, caused by selective saturation of the exchangeable protons.[49]

CEST agents can be roughly divided into paramagnetic and metal-free diamagnetic agents.[49,50] Diamagnetic CEST agents (DIACEST) include sugars, amino acids, nucleosides, indoles, pyrimidines and polymers with exchangeable protons. While these are exogenous agents, endogenous CEST (endo-

CEST) takes advantage on the endogenous molecules with exchangeable protons. These include for example some metabolites, proteins and peptides. The advantages of CEST are the possibility to detect several agents at the same time, and to study the micro-environment through their physico-chemical and biological parameters.

The other group of metal-free agents, hyperpolarized agents, are used mainly in studying metabolic pathways in cancer, cardiac diseases, and lung functions.[51] The method is based on hyperpolarizing the imaging agent before rapid administration to the subject.[52] The created hyperpolarized state, where the population of the spins in the lower and higher energy states is altered so, that the population in the lower energy state is considerably larger, significantly increases the sensitivity. Using this technique, also nonproton nuclei can be imaged.

Hyperpolarized agents are often divided into gases (^{3}He and ^{129}Xe) and liquid state (^{13}C and ^{15}N) agents. HP gases are used mainly for lung imaging.[53] Heteronuclei ^{13}C and ^{15}N are used as labels for different metabolites.[54] Examples of these metabolites comprise pyruvate, fumarate, dehydroascorbic acid—ascorbic acid (DHA—AA), bicarbonate, urea and glutamine. There are several hyperpolarization techniques: spin-exchange optical pumping (SEOP) and metastability exchange (ME) for gases, and dynamic nuclear polarization (DNP), parahydrogen-induced polarization (PHIP) and signal amplification by reversible exchange (SABRE) for liquids.

The downside of aforementioned methods is the need for special hardware. For example, using hyperpolarized agents, an external polarizing device is required. Another emerging group of metal-free contrast agents, nitroxyl radicals, can be readily applied for imaging with the existing routine techniques. Like metals, nitroxyl radicals are paramagnetic species and could provide a valuable addition to the metal-free imaging agents.

1.2 Nitroxyl radicals

Typically, radicals are considered as a highly reactive species. However, there are also stable and persistent radicals. Persistent radicals are often regarded as a species that can be observed with spectroscopic methods but are not stable enough to be isolated or handled in ambient conditions. Stable radicals, on the other hand, can be isolated, stored and used in chemical reactions without tethering the radical center. The most common groups of stable organic radicals include phenyl- hydrazyl- and nitroxyl radicals. Nitroxyl radicals, or nitroxides are probably the largest and most studied group of stable radicals. They are *N,N*-disubstituted N—O radicals with one unpaired electron delocal-

ized between the nitrogen and oxygen atoms. Nitroxides have a great variety of applications in organic synthesis,[55–59] polymerization,[60] and as spin labels,[61] molecular magnets,[62,63] and organic batteries.[64–68]

1.2.1 Nitroxides as metal-free contrast agents for MRI

Nitroxides were first studied as potential contrast agents for MRI already in the 1980s, simultaneously with the first GBCAs.[69–73] However, the nitroxides used at that time were not stable enough and seemed to reduce to diamagnetic hydroxylamines quite rapidly. Also, the relaxation effect given by GBCAs was much higher and they became the principal contrast agents. Since the development of MRI scanners and pulse sequences, and the search for metal-free contrast agents, the research of nitroxide-based contrast agents emerged in the 1990s, peaking its popularity in recent years. To overcome the issues of instability towards natural reductants and defective relaxivities, structural modifications have been the main thread in the research. The popularity of nitroxides as organic contrast agents can be accredited to the high stability and compact size of the molecules compared to other stable organic radicals, such as phenyl and hydrazyl radicals. Nitroxides act mainly as T_1 contrast enhancing agents, except for few examples.

1.2.1.1 Stability

Based on rapid bioreduction, nitroxides were initially considered suboptimal contrast agents for MRI.[74] Since then, extensive studies concerning nitroxide stability have been conducted and some consistencies in the structure-reactivity relationship have been found. Depending on the substituents in the α-position, instead of delocalizing between the nitrogen and the oxygen atoms, the unpaired electron can further delocalize in the whole structure, which destabilizes the radical. Also, hydrogens in the α-position markedly decrease the stability causing a disproportionation reaction between two nitroxide molecules to form a hydroxylamine and a nitrone. The mechanism has been proposed to follow a direct hydrogen atom abstraction[75] (pathway **a** in Scheme 1.2) or single electron transfer via head-to-tail-dimer through ion pair to proton transfer[76] (pathway **b**, Scheme 1.2) depending on the nitroxide structure.[77] There are also stable α-hydrogen nitroxides as presented in Scheme 1.3. These bridged bicyclic nitroxides are unable to form nitrones based on Brendt's rule.[78]

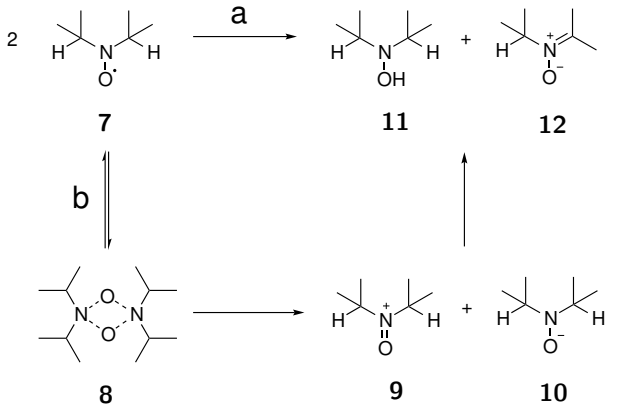

Scheme 1.2 Disproportionation mechanism for nitroxide with α-hydrogen. The reaction via direct hydrogen atom abstraction (**a**) and single electron transfer via head-to-tail-dimer through ion pair to proton transfer (**b**).

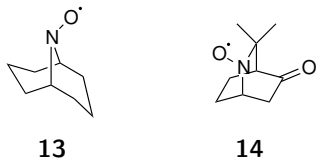

Scheme 1.3 Examples of stable nitroxides with α-hydrogen.

Nitroxides can undergo either oxidation or reduction reactions, both of which produce a diamagnetic, non-contrast enhancing equivalents of the radical form. The redox cycle of nitroxide radicals in Scheme 1.4 shows the one-electron oxidation and reduction of the radical **15**, to oxoammonium **16** and hydroxylamine **17**, respectively. In living organisms, reduction is the predominant process where the ascorbic acid and certain enzymes act as natural reductants. Oxidation process takes place mainly in the event of oxidative stress.[79]

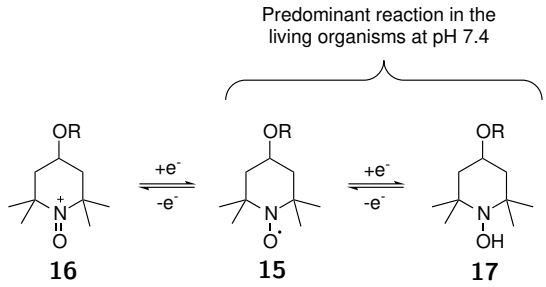

Scheme 1.4 Redox cycle of nitroxide radicals.[80]

In spite of the poor stability of the first nitroxide contrast agents, they seemed to have high potential and improving their stability became a common research objective.[81] The stability can be substantially improved by optimizing the structure. The structure–reactivity relationship is often assessed by measuring the redox potentials by cyclic voltammetry[82] or detecting the EPR (electron paramagnetic resonance) signal decay rate during the reaction between nitroxide and ascorbic acid.[83] These studies are often supported with computational methods, for instance geometry optimization[84] and SOMO–LUMO (singly occupied molecular orbital–lowest unoccupied molecular orbital) energy calculations.[85] The greatest single factor behind nitroxide stability is the size of its side groups in the α-position of the N—O moiety. The stability of the radical is proportional to the steric shielding provided by the side groups. According to reaction kinetic measurements, the shielding increases from *gem*-methyl to spirocyclohexyl to *gem*-ethyl (Scheme 1.5).[84]

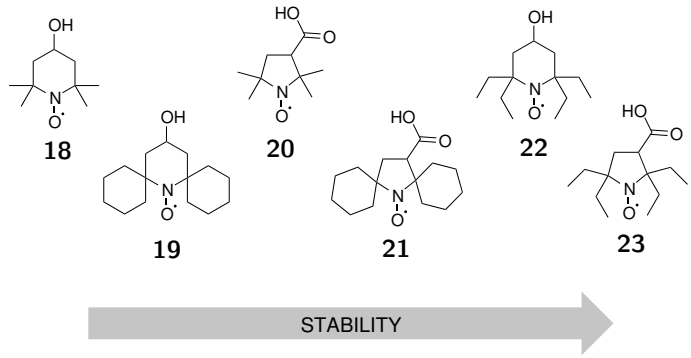

Scheme 1.5 The effect of the ring size and the side groups to the stability of different nitroxides.

According to the experimental data *gem*–diethyl groups provide more effective steric shielding to the nitroxide moiety than the spirocyclohexyl groups. Indeed, this can be confirmed for example with space-filling plots of the X-ray structures.[84] Furthermore, adding heteroatoms in the spiro rings reduces the stability as they can act as electron-withdrawing groups. This reduces the electron density around the nitroxide moiety, which favors the reduction.[85] Also, the ring size has an effect on the stability, 5-membered pyrrolidine being more stable than the 6-membered piperidine. The ring size seems to affect the accessibility of the reductant to the radical center.[86]

While optimizing the structure of a nitroxide-based contrast agent, there is a fine balance between stability and relaxivity. Some bulky side groups may increase the distance between the radical center and the water molecule so, that the efficiency of the relaxation enhancement decreases. On the other hand, the side groups should be large enough to prevent rapid bioreduction.

1.2.1.2 Functional modifications

By modifying the structures of the nitroxides, it is possible to create functional and more stable nitroxide contrast agents. For example, to image joints[87] and to detect proteoglycans in knee cartilage,[88] an ionic nitroxide (**24**, Scheme 1.6) was developed and used effectively. A contrast agent with improved water-solubility and stability towards reduction was constructed by adding NO-moiety to imidazol-4-yl 2-imidazoline (**25**).[89,90] Even more stable 4-oxo-TEEPO (4-oxo-2,2,6,6-tetraethylpiperidin-1-oxyl, **26**) radical was used for brain MR imaging as it proved to be able to cross healthy blood–brain barrier (BBB).[91]

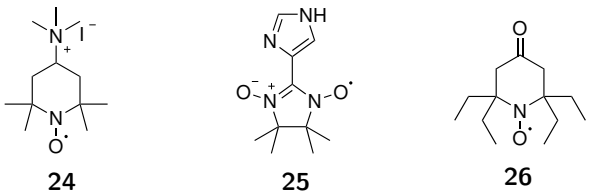

24 **25** **26**

Scheme 1.6 The structures of some nitroxide-based contrast agents.

Generally, small sized nitroxides can penetrate the BBB. This feature is important while imaging early-stage brain tumors with still intact BBB.[92] Also, these compounds offer a convenient method to study the BBB permeability of drugs, for instance. A study on the BBB permeability of a cancer drug lomustine (**27**, Scheme 1.7) was conducted by labeling the drug with a nitrox-

ide.[93,94] The distribution of the resulting compound SLENU (**28**) in mouse brain was detected with MRI as an improved T_1 relaxivity. The same agent was used to image cancer by detecting carcinogenesis with different redox activities between normal and cancer tissue.[80,95]

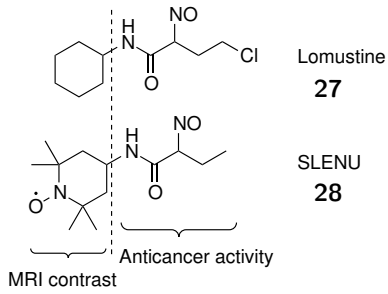

Scheme 1.7 The anticancer drug lomustine and corresponding MRI contrast enhancing nitroxide SLENU.

To construct small molecule tissue targeting agents, nitroxides have been attached to ibuprofen (**29**, Scheme 1.8) and ketoprofen (**30**).[96] These theranostic compounds were used for both therapeutic and diagnostic purposes acting as anti-inflammatory drugs and dual MRI/EPRI contrast agents, respectively. Mitochondria targeted mito-TEMPO (**31**) was used to study superoxide production in the dopaminergic area of the brain in Parkinson's disease[97] and mitochondrial dysfunction.[98]

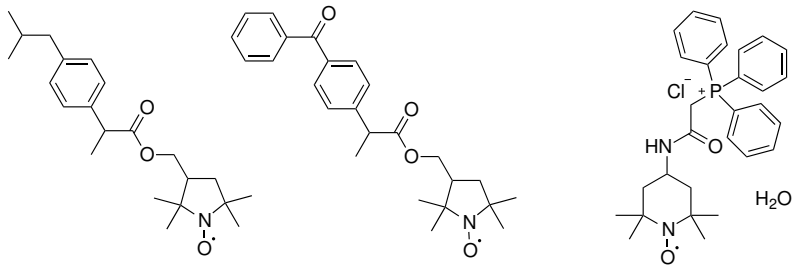

Scheme 1.8 The structures of ibuprofen and ketoprofen nitroxides, and mito-TEMPO.

A common technique to increase the relaxivity of nitroxide-based contrast agents is to reduce their tumbling and increase the rotational correlation time τ_R. The most obvious way to do so, is to enlarge the molecular size. Nitroxides

have been widely attached to natural and synthetic macromolecules that can act as an excellent backbone for different surface functionalities. They can also carry several nitroxide units to further increase the relaxivity. These macromolecules include for instance DNA oligomers,[99–101] viruses,[102] nanotubes,[103] self-asseblying polyradicals[104–107] and lyotropic liquid crystal nanoparticles.[108] There are also targeting macromolecular nitroxides possessing dual optical/MR imaging capabilities, like polyacetylene derivatives carrying folic acid and nitroxides,[109] and glucose functionalized fluorecent carbon quantum dots.[110]

Hyperbranched macromolecules, DAB (polypropylene imine)[111,112] and PAMAM (polyamidoamine)[113,114] dendrimers have also been linked to nitroxides. However, these compounds have relatively low relaxivities and poor water-solubility. The water-solubility can be increased by adding polyethylene glycol (PEG) groups to the structure. These PEG groups also immobilize nitroxides and improve the access of water molecules to the paramagnetic centers, causing more effective relaxation enhancement.[115]

Macrocyclic calix[4]arenes provide more rigid radical scaffold which improves τ_R. With suitable linkers, they provide positions for up to eight radical moieties producing for example tetra- and octaradicals (Scheme 1.9). In addition, the interactions between the unpaired electrons within the calix[4]arene structures improve the T_1 relaxation effect.[116] These interactions are through-bond and through-space exchange couplings and they occur in both 1,3-alternate (**32**) and cone (**33**) conformations (Scheme 1.9).[117] However, all couplings except through-bond exchange in cone are antiferromagnetic, thus 1,3-alternate conformation is preferred.[118] Other effective examples of rigid polymers carrying nitroxides include *N*-(2-Hydroxypropyl) methacrylamide (HPMA) copolymers,[119] polyacetylenes,[109] brush-arm star polymers (BASP),[120–122] heparin,[123] polyurethanes,[124] and hyperbranched polystyrene.[125]

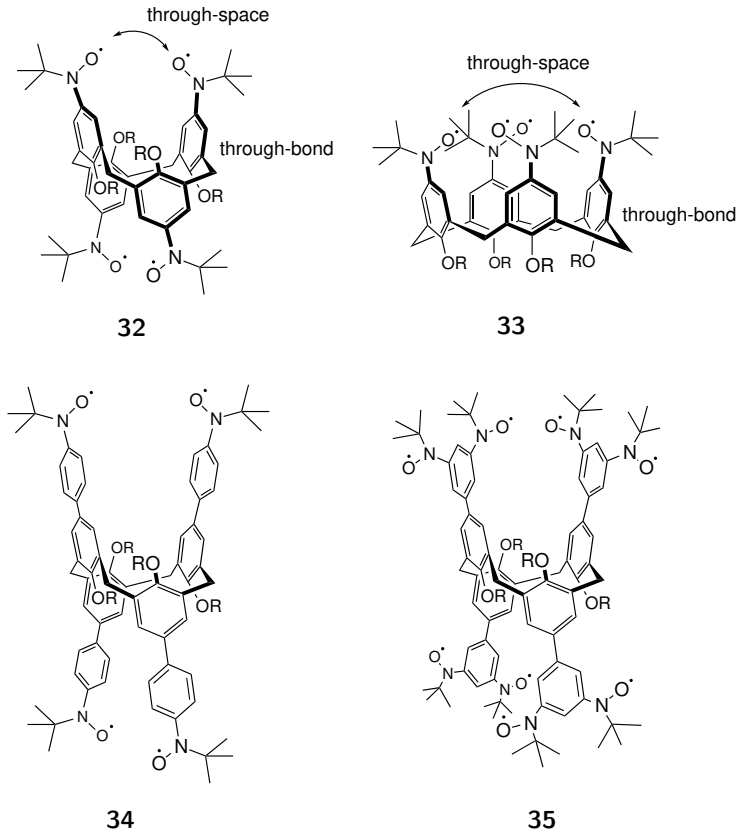

Scheme 1.9 Tetraradical and octaradical calix[4]arene nitroxides.

1.2.2 Electron paramagnetic resonance imaging of nitroxides

In addition to MRI, nitroxides can be used as electron paramagnetic resonance imaging (EPRI) probes. Electron paramagnetic resonance (EPR) is based on the same phenomenon as NMR, only instead of protons, the behaviour of electrons is monitored. Both protons and electrons are spinning charged particles, apart for the fact that electrons are in constant motion, inducing much larger dipole moment. As opposed to NMR, in EPR spectroscopy the frequency is kept constant, while the magnetic field is varied.

Nitroxides are commonly used as spin labels to study the structures and dynamics of macromolecules such as proteins with EPR spectroscopy.[126] Also, imidazolium based nitroxides can be used as pH-indicators due to their pH-sensitive protonation mechanism, which is observed as a change in the EPR spectrum.[127,128] It is also possible to image living organisms with EPR although it is still resticted to animals. EPR imaging is mostly used to study redox metabolism and hypoxia.[129–131] Also, the pharmacokinetics, such as

spreading and metabolism of spin labeled drugs, can be studied with EPRI.[132]

1.3 Magnetic resonance spectroscopy

In addition to producing anatomical images, biological tissues and their chemical compositions can be examined with NMR spectra *in vivo*. *In vivo* NMR, or better known as magnetic resonance spectroscopy (MRS), is used to study diseases based on changes in metabolites especially in the brain area.[133,134] These diseases include for instance brain tumors, epilepsy and stroke. Other possible targets for MRS are muscle, liver and prostate.[135,136] The most common nucleus measured with MRS is proton, ^{1}H, due to its high natural abundance and sensitivity.[137] Whereas in MRI the properties of water protons are detected, MRS is focused on the protons of metabolites, which are 10,000 times less concentrated.[138] Also, phosphorus ^{31}P, carbon ^{13}C, fluorine ^{19}F and sodium ^{23}Na spectroscopy are used in some extent. However, while in ^{1}H spectroscopy, standard RF coils and software can be used, non-proton spectroscopy requires special coils as well as other instrumentation such as preamplifiers matching them.

1.3.1 Metabolites

With ^{1}H MRS, a large number of biologically important metabolites can be detected and analyzed. The most common brain metabolites studied with MRS are lactate (Lac, **36**), *N*-acetyl aspartate (NAA, **37**), glutamate–glutamine (Glu–Gln, **38**), total creatine (tCr) comprising creatine (**39**) and phosphocreatine, choline containing compounds i.e. choline (Cho, **40**), phosphopcholine and glyserophosphocholine, and myo-inositol (mI, **41**) (Scheme 1.10). Each metabolite has its own function in living organisms (Table 1.2).

The absolute quantification of MR spectra is performed using a concentration reference.[139] The water signal can be used as an internal reference while an external reference is created with a phantom. Absolute quantification also requires the use of some signal correction factors like relaxation times. In clinical use, defining the relative concentrations is often sufficient. It is performed by comparing the intensities of the metabolite signals. The most common ratios under inspection in studies of neurological diseases are NAA/Cho, NAA/creatine and Cho/creatine. NAA often decreases in brain tumors and inflammatory processes whereas choline increases as it indicates myelin breakdown or rapid cell proliferation. Creatine is often used as a reference compound as its intensity hardly changes in most cases excluding brain tumors. To study hypoxia, lactate is often used as a reference due to its presence in anaerobic processes.

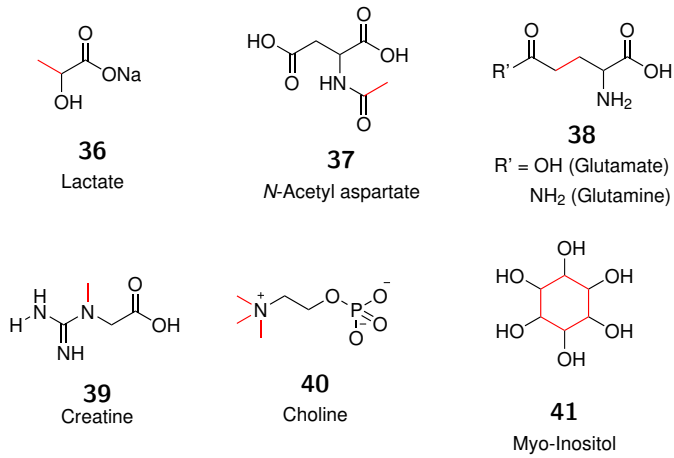

Scheme 1.10 Structures of the most common metabolites in brain detected with ^{1}H MR-spectroscopy. Red color indicates the molecular regions consisting of the protons responsible for characteristic signals listed in Table 1.2.

Table 1.2 Most common metabolites in brain ^{1}H spectroscopy.

Metabolite	ppm	c (mM)	Multiplicity	Function
Lac (**36**)	1.33	0.2-1	doublet	Anaerobic metabolite
NAA (**37**)	2.02	7.5-17	singlet	Neuron and axon marker
Glu-Gln (**38**)	2.05-2.50	6-12.5 (Glu) 3-6 (Gln)	multiplet	Neurotransmitters
creatine (**39**)	3.02	4.5-10.5	singlet	Energy metabolism
Cho (**40**)	3.22	0.5-2.5	singlet	Membrane marker
mI (**41**)	3.56	4-9	singlet	Glial marker

1.3.2 Techniques

Since metabolites appear at significantly lower intensities compared to water, water suppression techniques are essential in MRS. Water suppression is used to reduce the water signal appearing at 4.8 ppm and to obtain informative spectra. Also, in some cases fat suppression is needed to reduce the lipid resonances at 1.3 ppm. Probably the most common water suppression technique is CHEmical Shift-Selective (CHESS) sequence.[140] In the technique, frequency selective excitation pulses are used to rotate the water proton magnetization repeatedly into the transverse plane. Then, the magnetization is purged by application of pulsed field gradients. There are several variants of CHESS such as WET (Water suppression Enhanced Through T_1)[141] and VAPOR (VAriable Power pulses with Optimized Relaxation delays).[142]

There are two main options for spatial location in *in vivo* NMR: single voxel

spectroscopy (SVS) and chemical shift imaging (CSI), also referred as magnetic resonance spectroscopic imaging (MRSI). With SVS, a spectrum of a single volume element, voxel, is recorded from one specific location, whereas with CSI, a larger selected volume of interest (VOI) is monitored consisting of simultaneous excitation of many smaller voxels. While SVS is a more quantitative method, CSI produces metabolite maps offering information on distribution of various metabolites within the VOI. The most common sequences used with MRS are PRESS (Point Resolved Spectroscopy)[143] and STEAM (Stimulated Echo Acquisition Mode).[144] They both utilize three slice selective pulses to produce a spin echo or stimulated echo. In STEAM, three 90° pulses are used and in PRESS one 90° pulse is followed by two 180° pulses.

The advantage of PRESS is the high SNR (signal-to-noise) ratio, which is two times higher than the SNR obtained with STEAM. On the other hand, STEAM enables the use of very short TE. TE is often chosen according to the metabolites of interest, since using long TE only displays NAA, Cho, Cr and Lac signals while macromolecules and lipids decay to the noise level. Both sequences are commonly used, albeit PRESS is somewhat more common in clinical use.

2 Aims of the research

Noninvasive imaging is of vital importance in modern medical diagnostics. Magnetic resonance imaging (MRI) is a powerful tool especially when combined with contrast agents. Compared to the other common imaging methods, planar X-ray, CT and PET, the advantages of MRI are the lack of ionizing radiation, good soft tissue contrast and the broad accessibility of MRI imaging facilities. Due to the non-specificity and health-related issues associated with the widespread use of gadolinium-based contrast agents, a metal-free, tumor-targeting contrast agent would bring a substantial addition to the established MRI-based diagnostics. Therefore, the aims of the main part of the research were to develop stable nitroxide-based contrast agents with tumor targeting properties.

The second, smaller part of the research consisted of developing a tumor targeting marker compound for ^{1}H magnetic resonance spectroscopy and spectroscopic imaging (MRS and MRSI), methods applicable with MRI facilities. To the date, there are no targeting markers for MRS or MRSI.

Specifically, the aims of the research were:

1. to design and synthesize stable nitroxides conjugated with suitable targeting units to act as organic, metal-free contrast agents for MRI;
2. to assess their relaxation enhancing abilities with magnetic resonance studies *in vitro* and *in vivo*;
3. to design and synthesize an organic marker with potential tumor targeting moiety for MRS and MRSI;
4. to conduct *in vitro* and *in vivo* MRS and MRSI studies to assess the applicability of the compound as a tumor targeting marker for MRS/MRSI.

3 Methods

In general, the detailed analytical and experimental methods on synthesis and application studies of the radical contrast agents are described in publications I–III. The unpublished experimental methods for the study of the organic marker for MRS and MRSI are presented herein. Furthermore, the author participated in designing the study, performed the synthesis of the marker compound and its stability study, prepared the phantom and analyzed the results.

3.1 General methods

The blood plasma was purchased from the Finnish Red Cross Blood Service. The chemicals were acquired from commercial sources and used without further purification. The NMR spectra were recorded with a Varian Unity Inova 500 NMR-spectrometer (500 MHz ^{1}H-frequency, 11.7 T). The high-resolution mass spectroscopy (MS) was conducted with a Bruker Micro TOF with electron spray ionization (ESI).

3.2 Synthesis of TMSEt-Glc

2-(Trimethylsilyl)ethyl β-D-glucopyranoside (57): To a solution of 2-(Trimethylsilyl)ethyl 2,3,4,6-tetra-O-acetyl-β-D-glucopyranoside (**56**, 112 mg) in 1 ml of methanol was added 1 ml of 25 % NH_3 solution. The reaction mixture was stirred at room temperature for two hours. The excess solvent and NH_3 were removed in vacuo and the crude product was separated by silica gel column chromatography using 10 % MeOH / DCM as eluent yielding 2-(Trimethylsilyl)ethyl β-D-glucopyranoside **57** (70 mg, 99 %) as a white solid. ^{1}H NMR (500 MHz, D_2O): δ (ppm): 4.51 (d, ^{3}J=7.9 Hz, 1 H, *H*-1'), 4.05-4.11 (ddd, ^{3}J=5.2 Hz, ^{3}J=10.0 Hz, ^{2}J=-12.6 Hz, 1 H, CH_2), 3.94-3.97 (dd, ^{3}J=2.1 Hz, ^{2}J=-12.3 Hz, 1 H, *H*-6a'), 3.78-3.83 (ddd, ^{3}J=5.5 Hz, ^{3}J=10.1 Hz, ^{2}J=-12.4 Hz, 1 H, CH_2), 3.75-3.78 (dd, ^{3}J=5.6 Hz, ^{2}J=-12.3 Hz, 1 H, *H*-6b'), 3.52 (t, ^{3}J=9.0 Hz, 1 H, *H*-3'), 3.31-3.35 (ddd, ^{3}J=9.3 Hz, ^{3}J=5.6 Hz, ^{3}J=2.1 Hz,

1 H, *H*-5'), 3.43 (t, ^3J=9.3 Hz, 1 H, *H*-4'), 3.29 (t, ^3J=8.6 Hz, 1 H, *H*-2'), 1.09-1.15 (td, ^3J=5.5 Hz, ^2J=-12.9 Hz, 1 H, CH_2), 0.99-1.05 (td, ^3J=5.2 Hz, ^2J=-12.9 Hz, 1 H, CH_2), -0.08 (s, 9 H, CH_3). ^{13}C NMR (126 MHz, D_2O): δ (ppm): 104.32 (C-1'), 78.71 (C-3'), 78.67 (C-5'), 75.93 (C-2'), 72.41 (C-4'), 71.13 (CH_2), 63.53 (C-6'), 20.36 (CH_2), 0.30 (CH_3); MS (ESI) $C_{11}H_{24}O_6Si$: calc: 303.1234 $[M+Na]^+$, found: 303.1233 $[M+Na]^+$.

3.3 *In vitro* stability study

For the *in vitro* stability study, a 10 mM sample of TMSEt-Glc in blood plasma with 10 % of D_2O was prepared. The sample was incubated at 37 °C. The stability of TMSEt-Glc was monitored with Varian Unity Inova 500 NMR-spectrometer. Heteronuclear Multiple Bond Correlation (HMBC)[145] spectra were recorded after 1, 2, 3 and 24 hours of incubation.

3.4 Phantom study with MRS and MRSI

The phantom for the MRS and MRI study was constructed of TMSEt-Glc samples in buffered solution containing metabolites L-glutamine (9 mM), phosphocholine chloride calcium salt tetrahydrate (2 mM), myo-inositol (4 mM), sodium L-lactate (2 mM), *N*-acetyl aspartate (10 mM) and creatine (6 mM). The buffer solution (pH 7.2) contained K_2HPO_4 x 3 H_2O (72 mM), KH_2PO_4 (28 mM), Na-formate (200 mM) and NaN_3 (1 g/l). The phantom comprised seven NMR sample tubes (5 mm outer diameter) with TMSEt-Glc concentrations of 0 mM, 0.0625 mM, 0.125 mM, 0.25 mM, 0.5 mM, 1 mM, 2 mM.

The phantom was imaged with a vertical 9.4 T magnet. For the single voxel spectra, Point Resolved Spectroscopy (PRESS)[143] was used. Repetition time (TR) was 2 s, echo time (TE) 15 ms and spectral width (SW) 5020 Hz. For the water suppression VAPOR[142] (VAriable Power pulses with Optimized Relaxation delays) was used. The voxel size was 3x3x3 mm, the number of sampling points 4096 and the number of averages 256. For the chemical shift imaging (CSI) spin echo sequence was used with TR of 2 s and TE of 12 ms. A 4 mm slice was imaged with VAPOR water suppression, 4096 sampling points and 4 averages. The field of view (FOV) was 20x20 mm and the phase encoding matrix size 20x20.

4 Results and discussion

4.1 Organic radical contrast agents for MRI

Most of the traditional contrast agents for MRI lack selectivity and specificity. However, radiopharmaceutical chemistry has a long history with target-specific radiotracers.[146] In this study, this approach was used by connecting a relaxation enhancing nitroxide with tumor-targeting units producing potential contrast agents for MRI with specificity towards tumor tissue.

4.1.1 TEEPO-Glc and TEEPO-Met (I, II)

In the research, two nitroxides with potential contrast enhancing and tumor targeting properties were synthesized. The relaxation enhancing nitroxide moiety, TEEPO (2,2,6,6-tetraethylpiperidin-1-oxyl), was chosen based on its superior stability and relatively small size. The purpose of using a small radical moiety was to avert any attenuation of the possible targeting properties or blood-brain barrier permeability after attaching it to the targeting moiety. Additionally, while the bulky ethyl side groups provide effective steric shielding to the radical center, the distance between water molecule and paramagnetic center is short enough for an effective relaxation enhancement. For the targeting units, glucose (Glc) and methionine (Met) were selected owing to their increased uptake in tumors due to the proliferation of cancer cells.[147,148] Also, both have been succesfully applied as targeting radiotracers in PET.[149,150]

There are multiple published synthetic routes for 4-oxo-TEEPO, which acted as the precursor for further syntheses.[151–153] In this study, the approach via a pyrimidine intermediate was found the most suitable one (Scheme 4.1).[151] The multistep synthesis was initiated with a reaction of 2-ethylbutene (**42**) with chlorosulphonyl isocyanate to produce a β-lactam (**43**). After Boc protection (*tert*-butyloxycarbonyl), **44** was treated with methylmagnesiumbromide yielding a β-aminoketone (**45**) through Grignard reaction. The deprotection was performed with trifluoroacetic acid following a reaction with ammonia to

produce a pyrimidine (**46**). It was further treated with 3-pentenone and NH_4Br and the resulting piperidinone (**47**) was oxidized to produce the 4-oxo-TEEPO nitroxide (**26**).

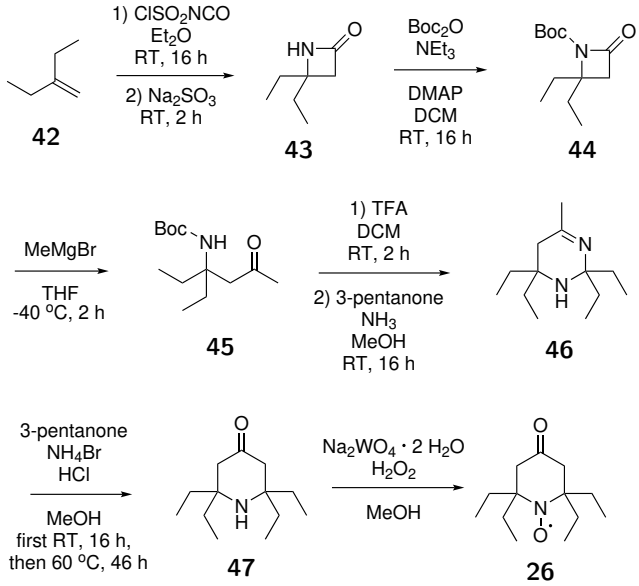

Scheme 4.1 Synthesis of 4-oxo-TEEPO **26** with reagents and conditions.

The conjugation of TEEPO to glucose was performed through glycosylation reaction using fluorinated glucose as the donor and boron trifluoride diethyl etherate as a Lewis acid (Scheme 4.2).[154] As for the acceptor, 4-oxo-TEEPO (**26**) was reduced to 4-hydroxy-TEEPO (**22**) with $NaBH_4$.[155] The fluorinated glucose compound (α-F-glucose) was prepared by treating β-D-glucose pentaacetate with HF pyridine.[156] The deacetylation of the glycosylated nitroxide (**48**) was performed with aqueous ammonia solution yielding the final product 2,2,6,6-tetraethylpiperidin-1-oxyl-4-yl-β-D-glucopyranoside (TEEPO-Glc, **49**).

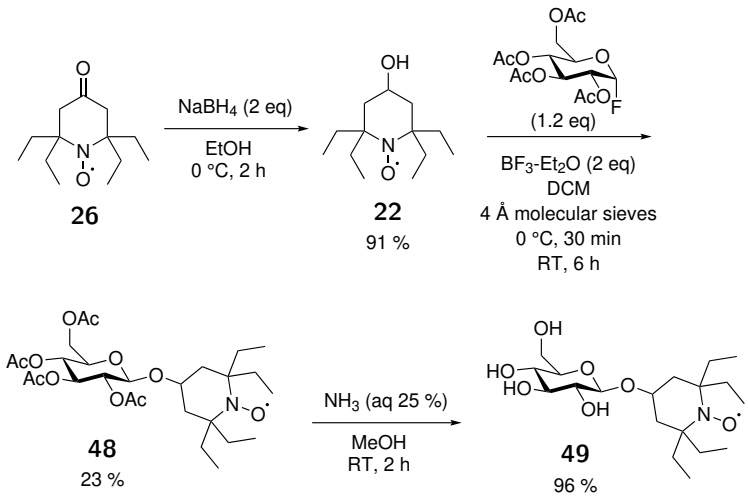

Scheme 4.2 Synthesis of TEEPO-Glc **49** with reagents and conditions.

TEEPO-Met was produced by attaching TEEPO to methionine through an amide bond. For the reaction, 4-oxo-TEEPO **26** was transformed via 4-carbonitrile-TEEPO **50** into 4-carboxy-TEEPO **51** .[157] In the coupling reaction, dicyclohexylcarbodiimide (DCC) was used as the activating agent in the presence of hydroxybenzotriazole (HOBt) hydrate and 4-methylmorpholine (NMM).[158] The reaction produced 4-[(L-methionine methyl ester)carbonyl]-2,2,6,6-tetraethylpiperidin-1-oxyl (TEEPO-Met-OMe, **52**) and the methyl ester protecting group was removed with NaOH yielding the final product TEEPO-Met **53**.

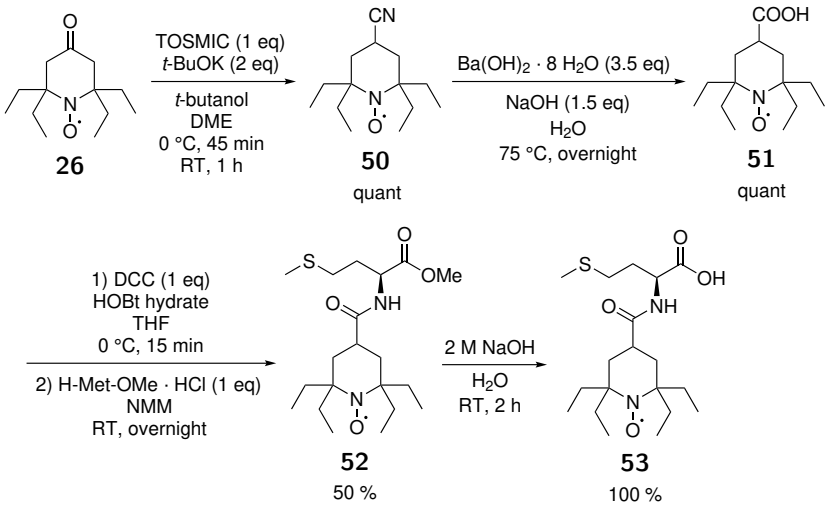

Scheme 4.3 Synthesis of TEEPO-Met **53** with reagents and conditions.

Also, less sterically shielded versions of the nitroxides were prepared as a reference for the stability studies. The TEEPO nitroxide moiety was replaced by TEMPO (2,2,6,6-tetramethylpiperidin-1-oxyl). The syntheses of TEMPO-Glc and TEMPO-Met followed the same procedure as for TEEPO-Glc and TEEPO-Met, respectively.

4.1.2 Stability towards reduction (I, II)

One of the most apparent concerns with radicals is their stability. Even though 4-oxo-TEEPO has proven to be stable,[84,85] the conjugation of nitroxide to a targeting unit may alter the radical stability.[159] To ensure the stability of the TEEPO-Glc and TEEPO-Met, NMR and EPR studies were conducted. The main threat to the nitroxide stability is its reduction to corresponding hydroxylamine by natural reductants, enzymes or antioxidants in human body. In this study, ascorbic acid was used in great excess (10 to 20-fold) to observe the reduction of the nitroxides to the corresponding hydroxylamines as these *in vitro* results correspond well to the lifetime of the radicals *in vivo*.[160]

The reduction of TEEPO-Glc was studied with NMR spectroscopy by monitoring the change of the water proton T_1 relaxation time. As the paramagnetic nitroxide reduces to diamagnetic hydroxylamine, it loses the ability to shorten the T_1 time of the nearby water protons and the relaxation time increases. As the reduction may be fast, a rapid relaxation measurement had to be used. Here, a method called Driven Equilibrium Single Pulse Observation of T_1 (DESPOT) was used.[161] In the method, two flip angles (θ_1 and θ_2) usually close to 45° and 90°, are used and the T_1 times are calculated using

these angle values, the repetition time (TR) and the signal integrals (I_1 and I_2) obtained from the aquisitions corresponding θ_1 and θ_2 (4.1).

$$T_1 = \frac{-TR}{\ln(\frac{I_1 \sin\theta_2 \cos\theta_1 - I_2 \sin\theta_1 \cos\theta_2}{I_1 \sin\theta_2 - I_2 \sin\theta_1})} \tag{4.1}$$

In the study, radical samples of TEEPO-Glc and TEMPO-Glc were prepared in D_2O with 1.6 % of H_2O and a 10-fold excess of ascorbic acid was added to the sample. As a result of a set of rapid T_1 measurements, TEEPO-Glc showed superior stability towards reduction. The relaxation enhancing properties of TEEPO-Glc remained effective for hours, whereas the less sterically protected nitroxide TEMPO-Glc was completely reduced after less than 10 minutes (Figure 4.1a).

The stability of TEEPO-Met was studied with EPR by detecting the the decrease in the signal intensity as the amount of paramagnetic nitroxide dropped. The TEEPO-Met and TEMPO-Met radical samples were prepared in phosphate buffered solution (PBS) corresponding to the pH of blood (7.4). The samples were treated with a 20-fold molar excess of ascorbic acid and the decay of high-field EPR peak height was monitored with respect to time. Again, TEEPO-Met showed good resistance towards reduction. After three hours only 10 % of TEEPO-Met was consumed in reductive conditions whereas TEMPO-Met was almost fully reduced in 10 minutes (Figure 4.1b).

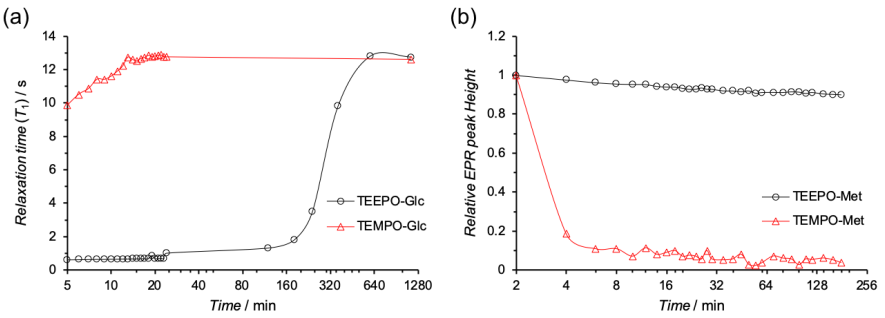

Figure 4.1 Reduction profiles of synthesized nitroxides. (a) The increase of water proton T_1 time of TEEPO-Glc (black circle) and TEMPO-Glc (red triangle) with respect to time measured with NMR spectroscopy in 11.7 T (500 MHz in ^{1}H frequency) field. (b) The decrease of EPR signal of TEEPO-Met (black circle) and TEMPO-Glc (red triangle) with respect to time.

The results confirmed the high stability of TEEPO-Glc and TEEPO-Met towards reduction especially compared to their TEMPO equivalents, which is in accordance with earlier studies on the stability of the nitroxide moieties.[84,85] The stability of nitroxides can be attributed mainly to the steric hindrance provided by the substituents adjacent to the radical centre. In summary, steric hindrance both prevents disproportionation of two nitroxides and block the access of reactive species to the radical centre.

4.1.3 Relaxometric studies in pre-clinical field (I, II)

The contrast effect in MRI is based on differences in relaxation times of different tissues. Contrast agents are used to enhance these differences by shortening the water proton T_1 relaxation time. The preliminary relaxometric studies of TEEPO-Glc and TEEPO-Met were performed with ^{1}H NMR spectroscopy in pre-clinical magnetic field (11.7 T) at 37 °C. The human blood plasma water relaxation times (T_1) and relaxation rates (R_1) were measured as a function of TEEPO-Glc and TEEPO-Met concentration. Both nitroxides conciderably shortened the T_1 and correspondingly increased the R_1 of water in human blood plasma (Figure 4.2). The TEEPO-Met samples contained 10 % of DMSO to improve the solubility, which may cause a stronger relaxation enhancement in those samples. With TEEPO-Glc, the T_1 relaxation time halved when the nitroxide concentration reached 2.5 mM, and further dropped to one third in 5 mM concentration. For TEEPO-Met, the respective concentration values were 2 and 4 mM. The R_1 rates increased linearly with the concentration, implying that the contrast agents show no aggregation in the concentration range studied.[115] The relaxivities (r_1) were defined by the slopes of the linear fits of R_1 as a function of concentration. The r_1 values were 0.12 mM^{-1} s^{-1} and 0.17 mM^{-1} s^{-1} for TEEPO-Glc and TEEPO-Met, respectively.

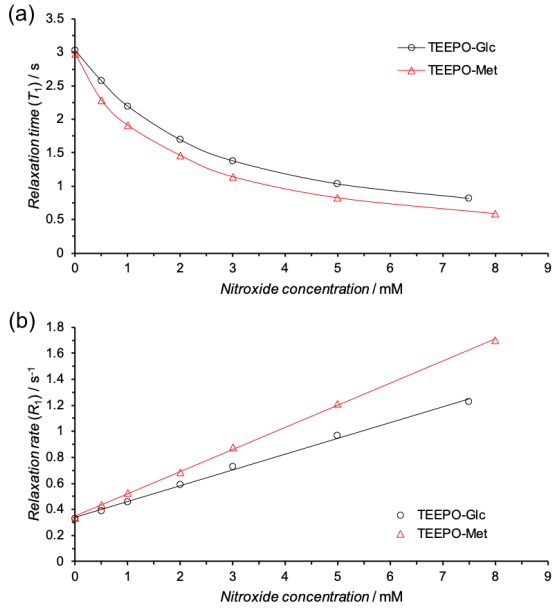

Figure 4.2 The blood plasma water T_1 relaxation times and R_1 relaxation rates measured in 11.7 T magnetic field (500 MHz ^{1}H frequency) at 37 °C in the presence of TEEPO-Glc and TEEPO-Met. (a) T_1 relaxation times as a function of TEEPO-Glc (black circle) and TEEPO-Met (red triangle) concentrations. (b) R_1 ($1/T_1$) relaxation rates as a function of TEEPO-Glc (black circle) and TEEPO-Met (red triangle) concentrations.

4.1.4 Phantom studies in clinical field (I, II)

To study the relaxation enhancing effect of the TEEPO-Glc and TEEPO-Met in clinical MRI magnetic field strength, phantoms consisting of several sample vials with varying nitroxide concentrations in human blood plasma were constructed and imaged with a 1.5 T clinical scanner. For TEEPO-Glc, concentrations of 0.2, 0.5, 1, 2, 5, 10 and 16 mM were selected for the phantom (Figure 4.3a). Also, as a reference, three samples of clinically used contrast agent, gadopentetate dimeglumine (Gd(DTPA)), were included in 0.01, 0.1 and 1 mM concentrations. The Gd(DTPA) concentrations were chosen to be significantly smaller compared to TEEPO-Glc as the relaxation effect is more effective with GBCAs mainly due to gadoliniums seven unpaired electrons in contrast to the one unpaired electron in TEEPO-Glc. From the T_1-weighted spoiled gradient echo fast low angle shot (FLASH) image (Figure 4.3b), it can be seen that the intensity difference between undoped and nitroxide-doped samples becomes visually detectable at a 0.5 mM concentration. Similar con-

centrations of nitroxides have been detected *in vivo* in previously studies.[162] The difference is even more pronounced in the colored T_1-weighted spoiled gradient echo image (Figure 4.3c) as well as T_1 and T_2 maps (Figure 4.3d-e).

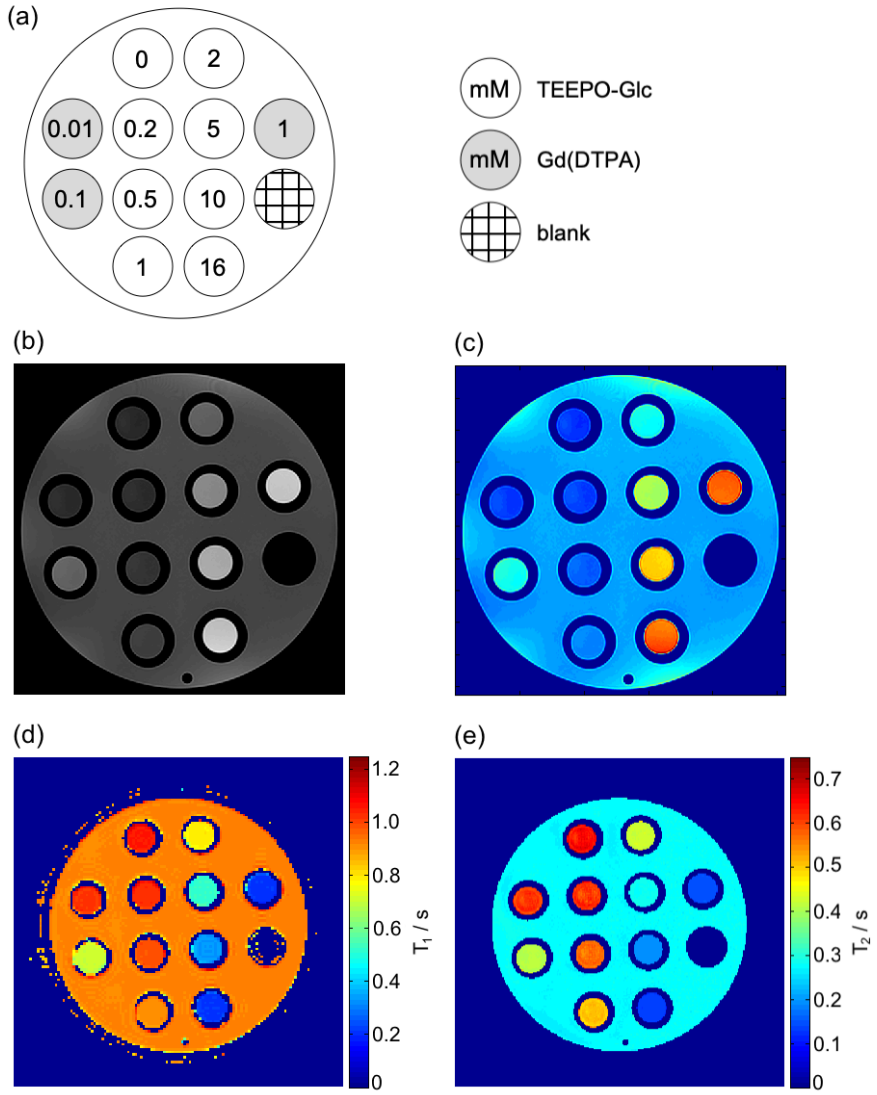

Figure 4.3 The phantom (200 mm diameter, 24 mm diameter vials) with TEEPO-Glc imaged with a 1.5 T clinical MRI scanner. (a) The composition of the phantom. (b) T_1-weighted spoiled gradient echo (FLASH) image (flip angle 90°, echo time 4.76 ms, repetition time 400 ms) in grey scale and (c) in color. (d) The inversion recovery T_1 and (e) multi-spin-echo T_2 maps of the phantom.

For TEEPO-Met, a small phantom comprising nitroxide in 10 % DMSO in blood plasma at concentrations of 0, 0.5, 1, 2, 5, 10 and 15 mM was constructed (Figure 4.4a). The small phantom imaged with a human-sized scanner caused some restrictions to the image quality which can be seen as a truncation artefact causing dark pixels in the centre of each sample tube in Figure 4.4b-c. In more detail, the artefact was caused by the low imaging resolution (0.8 mm / pixel) in contrast to the sample tube size (4 mm). Nevertheless, the results displayed a clear contrast between different concentrations. In T_1-weighted spoiled gradient FLASH image with a 90° pulse, a clear contrast between samples of undoped and nitroxide-doped samples can be seen (Figure 4.4b-c). This is also visible in T_1 and T_2 maps (Figure 4.4d-e).

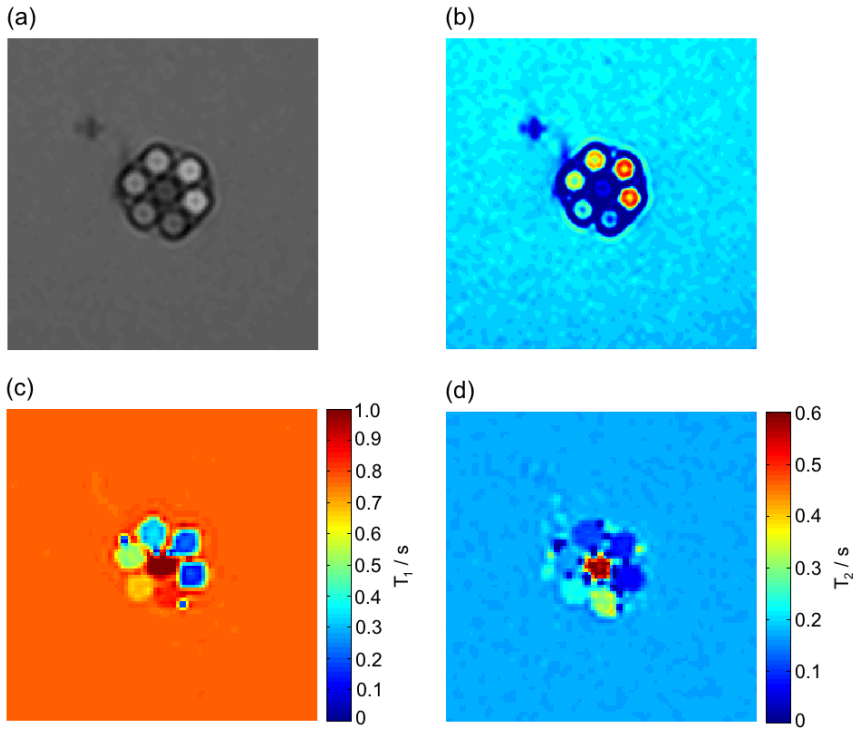

Figure 4.4 The phantom (4 mm inner diameter tubes in a 17 mm diameter spacer) with TEEPO-Met at concentrations of 0, 0.5, 1, 2, 5, 10 and 15 mM, imaged with a 1.5 T clinical MRI scanner. (a) T_1-weighted FLASH image (flip angle 90°, echo time 4.76 ms, repetition time 400 ms) in grey scale and (b) in color. (c) The inversion recovery T_1 and (d) multi-spin-echo T_2 maps of the phantom.

The relaxation times calculated from T_1 and T_2 maps showed similar results with the preliminary pre-clinical 11.7 T field strength studies (Figure 4.5) Relaxivities r_1 and r_2 in 1.5 T for TEEPO-Glc were 0.23 mM^{-1} s^{-1} and 0.38 mM^{-1} s^{-1}, respectively and for TEEPO-Met 0.31 mM^{-1} s^{-1} and 0.77 mM^{-1} s^{-1} (a rough estimate as the data is non-linear). Again, the DMSO used to improve the solubility of TEEPO-Met in blood plasma may cause a more effective relaxation enhancement for TEEPO-Met. These relaxivity values are in accordance with the values calculated for other monoradicals.[115,163]

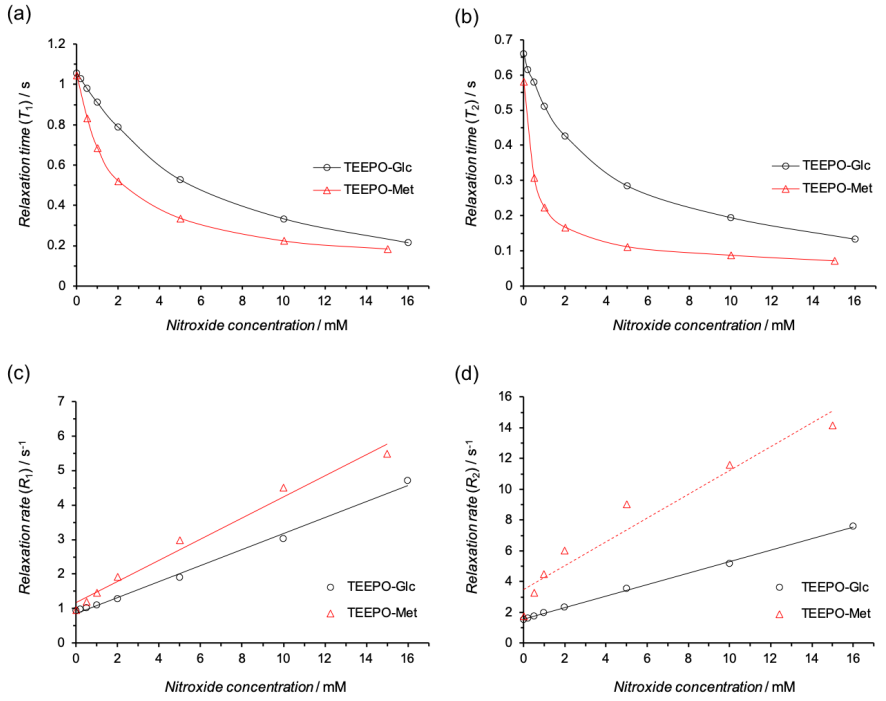

Figure 4.5 The blood plasma water relaxation times and rates in the presence of TEEPO-Glc and TEEPO-Met in 1.5 T magnetic field collected from the phantom study. (a) T_1 and (b) T_2 relaxation times as a function of TEEPO-Glc (black circle) and TEEPO-Met (red triangle) concentrations. (c) R_1 and (d) R_2 ($R_x = 1/T_x$) relaxation rates as a function of TEEPO-Glc (black circle) and TEEPO-Met (red triangle) concentrations.

Although the values are significantly lower than that of for example Gd-(DTPA) (r_1 4.1 mM^{-1} s^{-1} at 37 °C in 1.5 T),[29] the possible targeting effect could compensate this flaw by ensuring a sufficient concentration in the target tissue without extreme contrast agent dosing. Approximate ratio values r_2/r_1 for TEEPO-Glc and TEEPO-Met, 1.7 and 2.5, respectively, suggest that the

nitroxides could act mainly as T_1 contrast agents. T_1 contrast agents usually have r_2/r_1 ratio of 1-2, whereas the ratio for T_2 contrast agents is often 10 or higher.[19,44]

4.1.5 *In vitro* cytotoxicity (I, III)

One of the advantages of using nitroxides as potential contrast agents is their low toxicity.[93,120] The *in vitro* cytotoxicity of TEEPO-Glc was studied with cell viability and LDH release studies using two different cell lines, HeLa cells and HUVECs (human umbilical vein endothelial cells). To study the cell viability, the cells were treated with different amounts of TEEPO-Glc (0.2, 1 and 10 mM) and incubated for 1, 6 and 24 hours. The cell viability was determined using CellTiter-Glo® assay. The assay is based on quantitation of ATP (adenosine triphosphate) the amount of which is directly proportional to the number of living cells. According to the results, at a high concentration of TEEPO-Glc (10 mM) with long incubation time (24 h), the cell viability of HeLa cells decreased significantly ($p<0.05$) compared to unexposed controls (Figure 4.6a). However, toxicity was not observed at shorter incubation times (1 h and 6 h) or with smaller concentrations (0.2 mM and 1 mM) at any of the time points (1, 6 or 24 h). For HUVECs, TEEPO-Glc significantly reduced the cellular viability of cells exposed to a high concentration (10 mM) of TEEPO-Glc for 1h ($p<0.05$), 6 h ($p<0.05$) or 24 h ($p<0.05$) (Figure 4.6b). Nevertheless, low concentrations of TEEPO-Glc (0.2 mM or 1 mM) did not affect the cell viability.

The effect of TEEPO-Glc was also investigated by the LDH release assay, a colorimetric assay for the measurement of cytoplasmic LDH (lactate dehydrogenase) enzyme activity. LDH is rapidly released from the cytosol in culture medium upon damage of plasma membrane of the cells. The results from LDH assay showed that none of TEEPO-Glc treatments (0.2, 1 and 10 mM) caused a significant membrane the damage up to 24 h for the cultured HeLa cells (Figure 4.6c). With HUVECs, the highest concentration (10 mM) of TEEPO-Glc induced a significant LDH release ($p<0.05$) and loss of plasma membrane integrity for all the tested time points (1, 6 and 24 h) when compared to untreated control cells (Figure 4.6d). Lower concentrations of TEEPO-Glc did not show any membrane damaging effects at any of the time points tested. All in all, the TEEPO-Glc contrast agent showed toxicity only at a high 10 mM concentration and can be considered scarcely toxic in concentrations relevant for practical use.

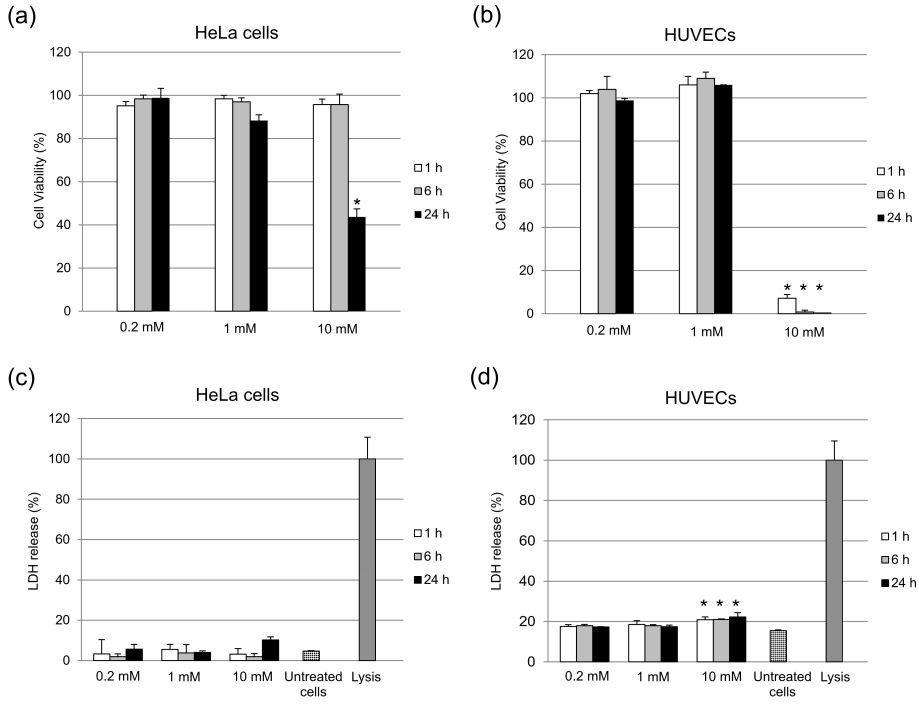

Figure 4.6 *In vitro* cytotoxicity of TEEPO-Glc. Cell viability study with (a) HeLa cells and (b) HUVECs determined by CellTiter-Glo® assay kit. The results (mean ± SD, n=4) were compared to untreated control cells with viability set at 100%. LDH release study with (c) HeLa cells and (d) HUVECs. Control cells were lysed with LDH assay lysis solution and set at 100% (Lysis). The level of significance was set at a probability of $p<0.05$ (*) when compared with untreated control cells (Kruskal-Wallis with Dunnett´s test).

4.1.6 *In vivo* animal MRI studies (III)

The relaxation enhancing properties of TEEPO-Glc were also assessed with an *in vivo* MRI study using Wistar rats. Unfortunately, solubility issues impeded the *in vivo* studies of TEEPO-Met. Neither saline doped with 10 % DMSO nor TWEEN20/80 produced a homogenous solution at the high concentration (150 - 200 mM) required for the study.

In the study, T_1 maps were collected before, during and after TEEPO-Glc injection with inversion recovery FLASH imaging sequence in 9.4 T magnetic field. Figure 4.7 shows results of a representative animal, that was given injections of TEEPO-Glc and Gd(DTPA) with a 60-minute time difference. By that time the first contrast agent had exited the tissue under study which was observed by the recovery of the relaxation time. Gd(DTPA) was used as a reference to compare the results of TEEPO-Glc to a common GBCA. Figure 4.7a displays two sets of T_1 images taken at approximately ten-minute intervals after TEEPO-Glc (top row) and Gd(DTPA) (bottom row) injections. The relaxation times were compared between two regions of interest (ROI): tumor (red area) and normal, healthy brain (blue area). Figure 4.7b presents the T_1 relaxation times in tumor and normal, healthy brain areas with respect to the time after the contrast agent injection. The values are voxel averages from within each region of interest (ROI) and the error bands represent their standard deviations (SD). The pre-injection relaxation time is longer in tumor that in normal brain due to the differences in the tissue type.

The results show a clear drop in the T_1 relaxation time in tumor after the TEEPO-Glc injection. The effect is strongest between 10 and 15 minutes resulting in a decrease of approximately 20 % in T_1. After 50 minutes, the T_1 relaxation time returns to the level of pre-injection T_1. In the healthy brain, no decrease in the T_1 relaxation times is detected. Compared to Gd(DTPA), TEEPO-Glc shows similar behavior in relation to retention and accumulation of the contrast agent. However, the relaxation effect is much higher with Gd(DTPA), supposedly due to the difference in the number of free electrons, Gd(DTPA) having seven unpaired electrons in contrast to TEEPO-Glc having one.

By contrast, the T_2 values in tumor were not affected by TEEPO-Glc even though they showed a good contrast in the previous phantom study. Similar to GBCAs, nitroxides seem to shorten both T_1 and T_2 times but the relative effect in tissue is much smaller for T_2 than for T_1 making them primarily T_1 contrast agents.

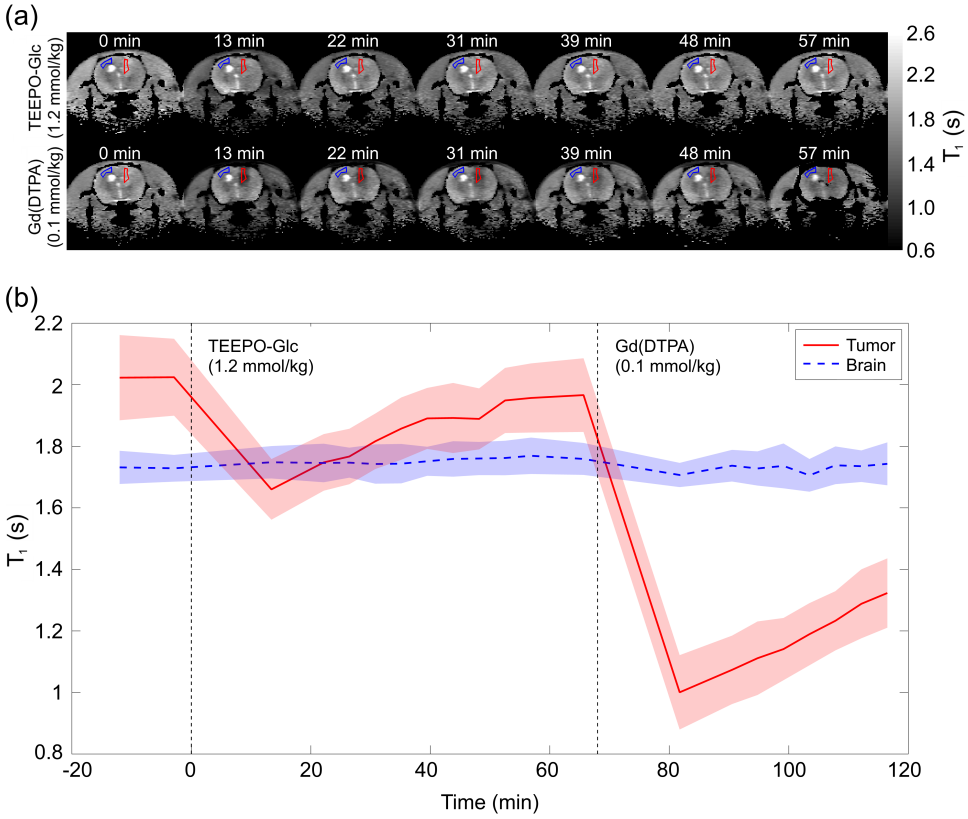

Figure 4.7 (a) T_1 images of rat brain taken approximately every 10 minutes after the TEEPO-Glc (top row) and Gd(DTPA) (bottom row) injections. The red and blue contours enclose the tumor and normal brain regions of interest (ROI), respectively. (b) The T_1 relaxation times within tumor and healthy brain ROI as a function of time from contrast agent injection with error bands (±SD).

Also, the apparent concentrations of TEEPO-Glc in tumor were studied. Table 4.1 presents the doses of TEEPO-Glc (animals 1–7) and Gd(DTPA) (animals 3 and 8–10) injected to each animal. The maximal contrast agent concentrations in tumor were calculated from the maximal R_1 rates and the r_1 values. The r_1 for TEEPO-Glc was determined to be 0.13 mM^{-1} s^{-1} at 9.4 T, which is in accordance with the values obtained in the earlier *in vitro* NMR and phantom MRI studies, 0.12 mM^{-1} s^{-1} at 11.7 T and 0.23 mM^{-1} s^{-1} at 1.5 T field. The concentrations were normalized with the injected TEEPO-Glc dose to give the %ID/g (percent of injected dose per gram of tissue) values (Table 4.1). According to the %ID/g values 0.19 ± 0.09 and 0.25 ± 0.09 for TEEPO-Glc and Gd(DTPA), respectively, the uptakes of the contrast agents are similar.

Table 4.1 Apparent contrast agent concentrations in tumor in each animal. The animal in bold (3) received both contrast agents.

	Animal	**Injected dose (µmol/g)**	**Injected dose (µmol)**	**Apparent tumor concentration (mM ∼ µmol/g)**	**%ID/g**
TEEPO-Glc	1	2.2	693	0.67	0.10
	2	1.6	615	0.85	0.14
	3	**1.2**	**385**	**0.83**	**0.22**
	4	1.2	285	0.59	0.21
	5	1.0	206	0.65	0.32
	6	1.0	210	0.48	0.23
	7	0.5	105	0.09	0.09
Average					0.19±0.08
Gd(DTPA)	**3**	**0.1**	**34**	**0.12**	**0.37**
	8	0.1	37	0.05	0.15
	9	0.1	37	0.09	0.24
	10	0.1	33	0.09	0.27
Average					0.25±0.09

The concentrations are presented with respect to the time from the injection in Figure 4.8. The values presented in the plot are averages of the animals presented in Table 4.1. According to Student's t-test, TEEPO-Glc exits the tumor at a faster rate than Gd(DTPA) ($p<0.01$). The mean lifetimes were 23 ± 8 min and 49 ± 10 min for TEEPO-Glc and Gd(DTPA), respectively. The rapid clearance and the similar uptake of the contrast agents may suggest low targeting effect of TEEPO-Glc. The targeting effect could be further studied using the radical moiety, 4-hydroxy-TEEPO, as a reference contrast agent. However, due to its high lipophilicity, it was insoluble in pure saline or saline doped with 10 % DMSO or TWEEN20/80 at desired concentrations.

Additionally, the less lipophilic equivalent of 4-hydroxy-TEEPO, 4-hydroxy-TEMPO, showed rapid bio-reduction losing its paramagnetism and ruling it out as a reference.

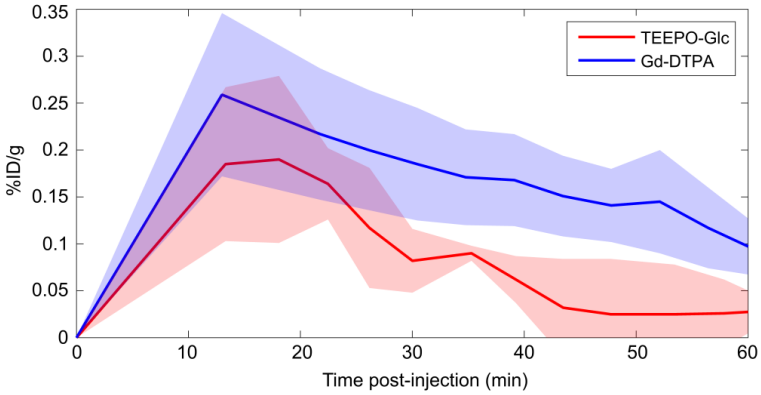

Figure 4.8 The apparent concentration of TEEPO-Glc and Gd(DTPA) in tumor as a function of time from TEEPO-Glc injection with error bands (±SD).

4.2 Organic marker for MRS and MRSI

Magnetic resonance spectroscopy (MRS) and imaging (MRSI) are used to study the metabolism *in vivo*. To our knowledge, there are no MRS / MRSI markers targeted for specific tissue metabolism currently available. Usually, the information on aberrations in metabolism are diagnosed by observing the metabolite signal intensities and by comparing them with the intensities in healthy tissue or their relation to other metabolite intensities. In healthy brain, the metabolite signals are usually located at 0.5-5.0 ppm in ^{1}H MRS spectrum. In this study, a marker consisting of glucose labeled with trimethylsilyl (TMS) group was developed. Trimethylsilyl group is usually detected close to 0 ppm in ^{1}H spectrum, an area where no natural metabolites appear. Glucose could potentially act as a targeting moiety towards the increased metabolism in tumor tissue. Consequently, a signal at 0 ppm in ^{1}H spectrum would suggest an increased uptake of glucose in the area under investigation, and a potential tumor finding and characterization.

4.2.1 TMSEt-Glc

In the study, glucose unit (Glc) was used as a potential targeting unit due to its superior water solubility and its fuction as brain energy source. It was labeled with TMS group via an ethyl bridge in order to bring the ^{1}H NMR signal of the TMS groups closer to 0 ppm. For the synthesis, peracetylated glucose **54** was treated with hydrogen bromide solution (33 % in AcOH) (Scheme 4.4). The resulting α-acetobromoglucose **55** was used as a donor in the reaction with 2-TMS-ethanol as acceptor, with AgOTf (silver trifluoromethanesulfonate) and 2,4,6-trimethylpyridine activation.[164] Deacetylation of **56** was performed by stirring the compound with 25 % ammonia solution in methanol at room temperature yielding TMSEt-Glc (2-(trimethylsilyl)ethyl β-D-glucopyranoside) **57** as the final product.

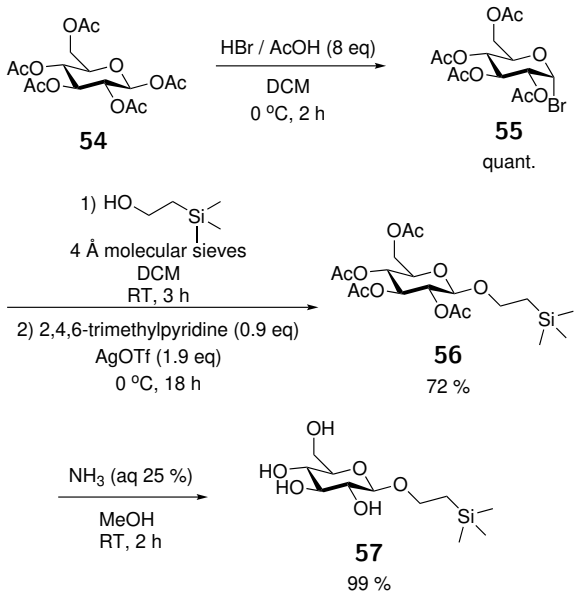

Scheme 4.4 Synthesis of TMSEt-Glc **57** with reagents and conditions.

4.2.2 Stability towards dissociation

The possible undesired transformation of TMSEt-Glc is the dissociation to glucose and TMSEtOH. The most propable mechanism for this process *in vivo* is hydrolysis of the glycosidic bond (Scheme 4.5) catalysed by glycosidase enzyme. The anomeric conformation of the resulting glucose is enzyme dependent.[165]

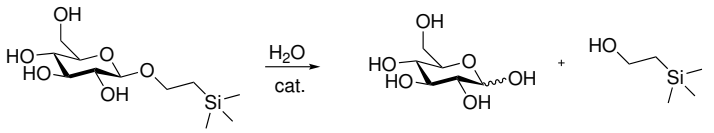

57 **58** **59**

Scheme 4.5 Dissociation of TMSEt-Glc **57** to glucose **58** and TMSEtOH **59** by glycosidic bond hydrolysis.

The stability of the glycosidic bond in TMSEt-Glc was evaluated by a simple *in vitro* stability test. The compound was incubated at a 10 mM concentration in human blood plasma at 37 °C for 1, 2, 3 and 24 hours and the potential dissociation reaction was monitored with NMR spectroscopy by HMBC[145] (Heteronuclear Multiple Bond Correlation) experiment. In the spectra, a correlation between the anomeric proton *H*-1' (4.41 ppm) of the glucose moiety and $-CH_2$-carbon (71.10 ppm) of the ethyl-TMS moiety can be clearly detected even after 24 hours (Figure 4.9). This result suggests that the compound is stable and does not go through dissociation reaction in biological matrix and conditions similar to living organisms.

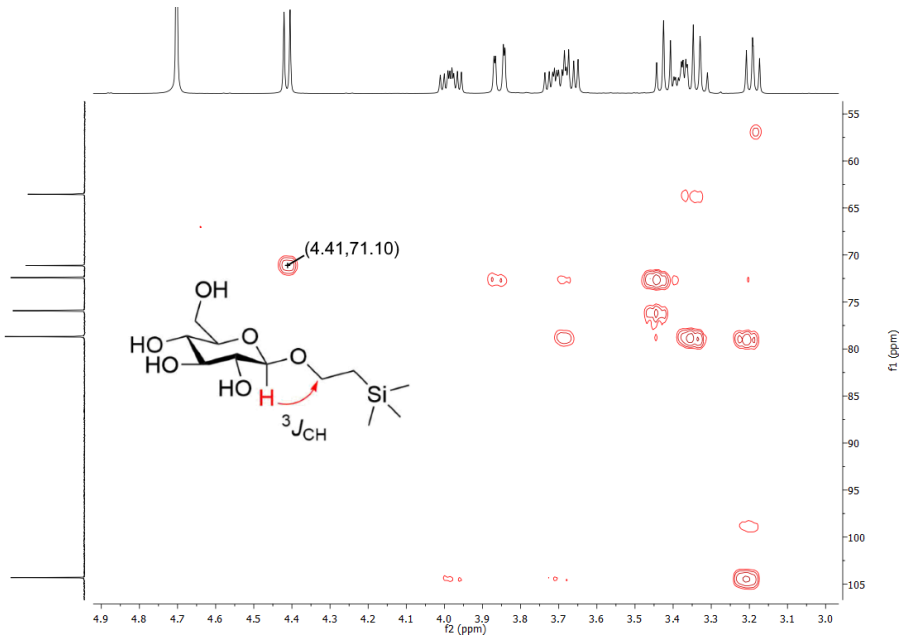

Figure 4.9 The HMBC spectrum of TMSEt-Glc in human blood plasma with 10 % of D_2O. A clear correlation between *H*-1' and $-CH_2$ can be seen.

4.2.3 Spectroscopic phantom studies

To study the TMSEt-Glc as a potential marker for MRS and MRSI, a phantom was constructed and imaged in 9.4 T magnetic field. The phantom consisted of varying concentration of TMSEt-Glc (0.0625 mM, 0.125 mM, 0.25 mM, 0.5 mM, 1 mM, 2 mM) in a buffered solution containing various common metabolites to imitate a biological matrix. The metabolites used in the study were lactate (Lac), *N*-acetyl aspartate (NAA), glutamine (Gln), creatine, choline (Cho) and myo-inositol (mI). From a single voxel MRS spectrum in Figure 4.10 it can be seen that the TMS-signal of TMSEt-Glc becomes visible at a concentration of 0.125 mM with *in vitro* conditions. After the concentration reaches 0.5 mM, the signal is clearly visible compared to some of the metabolites with higher concentration such as lactate (2 mM) glutamine (9 mM) or creatine (6 mM). That is due to the large number of protons in the TMS group consisting of three $-CH_3$ groups appearing as a singlet at 0 ppm in the spectrum.

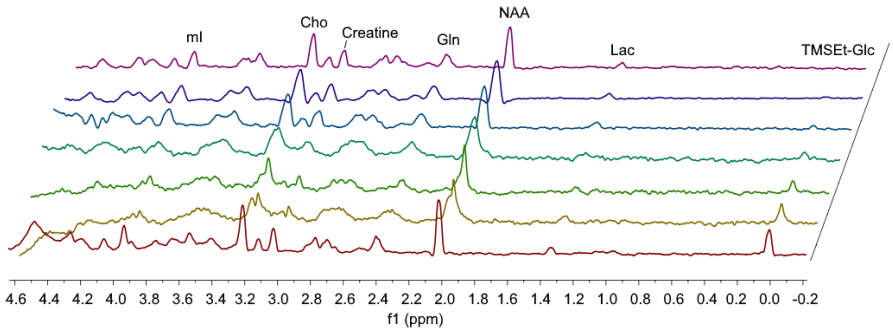

Figure 4.10 MRS spectra of TMSEt-Glc at concentrations of 0.0625 mM, 0.125 mM, 0.25 mM, 0.5 mM, 1 mM and 2 mM in a buffered solution doped with most common metabolites. The TMSEt-Glc concentration is increasing from top to bottom.

In addition to single voxel MRS, a chemical shift imaging (CSI) was performed to obtain MRSI color maps of the phantom metabolites. The color maps obtained from integrations of TMSEt-Glc and NAA signals are presented in Figure 4.11. As expected, the distribution of TMSEt-Glc varies in proportion to the concentration (Figure 4.11b). Also, an uniform distribution of NAA can be distinguished as all the sample tubes contain the same amount of NAA (Figure 4.11c). Altogether, an increase similar to results with ^{1}H MRS in signal intensity can be seen as the concentration of TMSEt-Glc becomes larger.

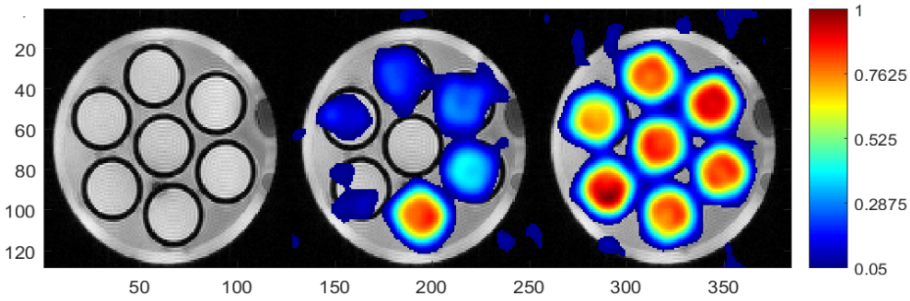

Figure 4.11 Chemical shift imaging of the phantom (4 mm inner diameter tubes in a 17 mm diameter spacer) in 9.4 T magnetic field. Color maps obtained from integration of TMSEt-Glc (center) and NAA signals (right) overlaid on gradient echo MR image (left). The integration regions were -0.2–0.1 and 1.9–2.2 for TMSEt-Glc and NAA, respectively.

Disappointingly, the *in vivo* animal ^{1}H MRS studies with Wistar rats showed no traces of TMSEt-Glc in the tumor area or in the brain area. The reasons for this could not be defined. According to the stability test, it is unlikely that the compound dissociates *in vivo*. It is possible that the concentration required for a detectable signal could not be reached in the area under investigation.

5 Conclusions

In this study, two stable, metal-free nitroxides with contrast enhancing abilities were developed. The compounds comprised a paramagnetic nitroxide moiety TEEPO and a glucose (Glc) or methionine (Met) moiety designed to act as a potential targeting unit. The stability of the resulting TEEPO-Glc and TEEPO-Met towards reduction by a natural reductant, ascorbic acid, was evaluated by using NMR and EPR-spectroscopy, respectively. Both of the compounds displayed superior stability, which is directly proportional to the size of the steric hindrance provided by the side groups adjacent to the radical center. Their effect on the relaxation times of the surrounding water protons were assessed in both pre-clinical (11.7 T) and clinical (1.5 T) fields with *in vitro* NMR and phantom MRI studies. Both TEEPO-Glc and TEEPO-Met showed relaxation enhancing properties having r_1 values of 0.12 mM^{-1} s^{-1} and 0.17 mM^{-1} s^{-1} in pre-clinical filed, and 0.23 mM^{-1} s^{-1} and 0.31 mM^{-1} s^{-1} in clinical field, respectively. The applicability of TEEPO-Glc as an MRI contrast agent was also assessed with a *in vivo* animal MRI study in 9.4 T field. The study gave similar results with the *in vitro* studies, i.e. TEEPO-Glc was able to shorten T_1 relaxation time also *in vivo*. Although the results of the phantom study indicated that TEEPO-Glc also reduces the T_2 relaxation time of nearby water protons, the *in vivo* animal study showed no shortening in the T_2 relaxation time. Consequently, a water soluble metal-free contrast agent with similar behaviour to Gd(DTPA), concerning accumulation and relaxation enhancement in the tumor area, was confirmed. The relaxation enhancement was obviously smaller for TEEPO-Glc, due to the higher amount of unpaired electrons in Gd(DTPA). Unfortunately, the targeting effects could not be assessed with this study. Also, improving the water solubility of TEEPO-Met at high concentrations requires further attention. According to these results, TEEPO-based compounds conjugated with targeting units show potential as T_1 contrast agents for MRI.

Furthermore, an organic marker for magnetic resonance spectroscopy and spectroscopic imaging was designed. The marker consisted of a tumor targeting

unit, glucose, labelled with a TMS-group. According to the results of a spectroscopic phantom study, the compound gave a considerably large signal with a relatively low concentration. Also, the signal appeared at 0 ppm, a spectral region where no natural metabolites appear. Disappointingly, the *in vivo* animal studies showed no traces of the marker in any area of the research subject. According to an *in vitro* stability study, no dissociation of TMS from the glucose moiety should occur in biological matrix indicating that additional work is required to work out the root cause for the invisibility of the signal.

Bibliography

[1] I. I. Rabi, J. R. Zacharias, S. Millman, P. Kusch. A New Method of Measuring Nuclear Magnetic Moment. *Physical Review* **1938**, *53*, 318–318.

[2] E. M. Purcell, H. C. Torrey, R. V. Pound. Resonance Absorption by Nuclear Magnetic Moments in a Solid. *Physical Review* **1946**, *69*, 37–38.

[3] F. Bloch. Nuclear induction. *Physics Today* **1950**, *3*, 22–25.

[4] R. Damadian. Tumor Detection by Nuclear Magnetic Resonance. *Science* **1971**, *171*, 1151–1153.

[5] R. Damadian, Apparatus and method for detecting cancer in tissue., US3789832, **1974**.

[6] P. C. Lauterbur. Image Formation by Induced Local Interactions: Examples Employing Nuclear Magnetic Resonance. *Nature* **1973**, *242*, 190–191.

[7] P. Mansfield, A. A. Maudsley. Medical imaging by NMR. *The British Journal of Radiology* **1977**, *50*, 188–194.

[8] R. de Graaf, *In Vivo NMR Spectroscopy: Principles and Techniques*, John Wiley & Sons, **2013**.

[9] N. Bloembergen, E. M. Purcell, R. V. Pound. Relaxation Effects in Nuclear Magnetic Resonance Absorption. *Physical Review* **1948**, *73*, 679–712.

[10] I. Solomon. Relaxation Processes in a System of Two Spins. *Physical Review* **1955**, *99*, 559–565.

[11] N. Bloembergen. Proton Relaxation Times in Paramagnetic Solutions. *The Journal of Chemical Physics* **1957**, *27*, 572–573.

[12] N. Bloembergen, L. O. Morgan. Proton Relaxation Times in Paramagnetic Solutions. Effects of Electron Spin Relaxation. *The Journal of Chemical Physics* **1961**, *34*, 842–850.

[13] H. Friebolin, *Basic One- and Two-Dimensional NMR Spectroscopy*, John Wiley & Sons, **1998**.

[14] D. W. McRobbie, *MRI from Picture to Proton*, Cambridge University Press, **2006**.

[15] B. K. H. Jeremy K. M. Sanders, *Modern NMR Spectroscopy: A Guide for Chemists*, Oxford University Press, **1993**.

[16] G. M. Clore, J. Iwahara. Theory, Practice, and Applications of Paramagnetic Relaxation Enhancement for the Characterization of Transient Low-Population States of Biological Macromolecules and Their Complexes. *Chemical Reviews* **2009**, *109*, 4108–4139.

[17] R. B. Lauffer. Paramagnetic metal complexes as water proton relaxation agents for NMR imaging: theory and design. *Chemical Reviews* **1987**, *87*, 901–927.

[18] A. D. Sherry, Y. Wu. The importance of water exchange rates in the design of responsive agents for MRI. *Current Opinion in Chemical Biology* **2013**, *17*, 167–174.

[19] P. Caravan, J. J. Ellison, T. J. McMurry, R. B. Lauffer. Gadolinium(III) Chelates as MRI Contrast Agents: Structure, Dynamics, and Applications. *Chemical Reviews* **1999**, *99*, 2293–2352.

[20] V. C. Pierre, M. J. Allen, P. Caravan. Contrast agents for MRI: 30 years and where are we going? *JBIC Journal of Biological Inorganic Chemistry* **2014**, *19*, 127–131.

[21] L. M. D. León-Rodríguez, A. F. Martins, M. C. Pinho, N. M. Rofsky, A. D. Sherry. Basic MR relaxation mechanisms and contrast agent design. *Journal of Magnetic Resonance Imaging* **2015**, *42*, 545–565.

[22] H. Gries, D. Rosenberg, H.-J. Weinmann, Use of paramagnetic complex salts for the preparation of agents for NMR diagnostics., DE3129906, **1983**.

[23] E. Fobben, G. L. Wolf. Gadolinium DTPA -A Potential NMR Contrast Agent. Effects Upon Tissue Proton REelaxation and Cardiovascular Function in the Rabbit. *Investigative Radiology* **1983**, *18*, S6.

[24] H. Weinmann, R. Brasch, W. Press, G. Wesbey. Characteristics of Gadolinium-DTPA Complex: a Potential NMR Contrast Agent. *American Journal of Roentgenology* **1984**, *142*, 619–624.

[25] G. L. Wolf, E. S. Fobben. The Tissue Proton T_1 and T_2 Response to Gadolinium DTPA Injection in Rabbits. A Potential Renal Contrast Agent for NMR Imaging. *Investigative Radiology* **1984**, *19*, 324–328.

[26] V. Runge, J. Clanton, C. Lukehart, C. Partain, A. James. Paramagnetic agents for contrast-enhanced NMR imaging: a review. *American Journal of Roentgenology* **1983**, *141*, 1209–1215.

[27] H. Gries, D. Rosenberg, H.-J. Weinmann, Diagnostic media., US4647447, **1987**.

[28] A. D. Sherry, P. Caravan, R. E. Lenkinski. Primer on gadolinium chemistry. *Journal of Magnetic Resonance Imaging* **2009**, *30*, 1240–1248.

[29] M. Rohrer, H. Bauer, J. Mintorovitch, M. Requardt, H.-J. Weinmann. Comparison of Magnetic Properties of MRI Contrast Media Solutions at Different Magnetic Field Strengths. *Investigative Radiology* **2005**, *40*, 715–724.

[30] T. Grobner. Gadolinium – a specific trigger for the development of nephrogenic fibrosing dermopathy and nephrogenic systemic fibrosis? *Nephrology Dialysis Transplantation* **2006**, *21*, 1104–1108.

[31] P. Marckmann, L. Skov, K. Rossen, A. Dupont, M. B. Damholt, J. G. Heaf, H. S. Thomsen. Nephrogenic Systemic Fibrosis: Suspected Causative Role of Gadodiamide Used for Contrast-Enhanced Magnetic Resonance Imaging. *Journal of the American Society of Nephrology* **2006**, *17*, 2359–2362.

[32] B. Wagner, V. Drel, Y. Gorin. Pathophysiology of gadolinium-associated systemic fibrosis. *American Journal of Physiology-Renal Physiology* **2016**, *311*, F1–F11.

[33] I. M. Braverman, S. Cowper. Nephrogenic systemic fibrosis. *F1000 Medicine Reports* **2010**, *2*, 84.

[34] T. Kanda, K. Ishii, H. Kawaguchi, K. Kitajima, D. Takenaka. High Signal Intensity in the Dentate Nucleus and Globus Pallidus on Unenhanced T_1-weighted MR Images: Relationship with Increasing Cumulative Dose of a Gadolinium-based Contrast Material. *Radiology* **2014**, *270*, 834–841.

[35] T. Kanda, T. Fukusato, M. Matsuda, K. Toyoda, H. Oba, J. Kotoku, T. Haruyama, K. Kitajima, S. Furui. Gadolinium-based Contrast Agent Accumulates in the Brain Even in Subjects without Severe Renal Dysfunction: Evaluation of Autopsy Brain Specimens with Inductively Coupled Plasma Mass Spectroscopy. *Radiology* **2015**, *276*, 228–232.

[36] T. Kanda, Y. Nakai, S. Aoki, H. Oba, K. Toyoda, K. Kitajima, S. Furui. Contribution of metals to brain MR signal intensity: review articles. *Japanese Journal of Radiology* **2016**, *34*, 258–266.

[37] T. Taoka, S. Naganawa. Gadolinium-based Contrast Media, Cerebrospinal Fluid and the Glymphatic System: Possible Mechanisms for the Deposition of Gadolinium in the Brain. *Magnetic Resonance in Medical Sciences* **2018**, *17*, 111–119.

[38] FDA Drug Safety Communication: FDA Warns that Gadolinium-Based Contrast Agents (GBCAs) are Retained in the Body; Requires New Class Warnings. Available online: https://www.fda.gov/Drugs/DrugSafety/ucm589213.htm (accessed on 13 May 2019).

[39] Referral: Gadolinium-containing contrast agents. Available online: https://www.ema.europa.eu/en/medicines/human/referrals/gadolinium-containing-contrast-agents (accessed on 13 May 2019).

[40] L. Telgmann, M. Sperling, U. Karst. Determination of gadolinium-based MRI contrast agents in biological and environmental samples: A review. *Analytica Chimica Acta* **2013**, *764*, 1–16.

[41] J. Rogowska, E. Olkowska, W. Ratajczyk, L. Wolska. Gadolinium as a new emerging contaminant of aquatic environments. *Environmental Toxicology and Chemistry* **2018**, *37*, 1523–1534.

[42] S. Kulaksız, M. Bau. Anthropogenic gadolinium as a microcontaminant in tap water used as drinking water in urban areas and megacities. *Applied Geochemistry* **2011**, *26*, 1877–1885.

[43] D. Pan, A. H. Schmieder, S. A. Wickline, G. M. Lanza. Manganese-based MRI contrast agents: past, present, and future. *Tetrahedron* **2011**, *67*, 8431–8444.

[44] G. Huang, H. Li, J. Chen, Z. Zhao, L. Yang, X. Chi, Z. Chen, X. Wang, J. Gao. Tunable T_1 and T_2 contrast abilities of manganese-engineered iron oxide nanoparticles through size control. *Nanoscale* **2014**, *6*, 10404–10412.

[45] J. W. M. Bulte, D. L. Kraitchman. Iron oxide MR contrast agents for molecular and cellular imaging. *NMR in Biomedicine* **2004**, *17*, 484–499.

[46] Y.-X. J. Wang. Superparamagnetic iron oxide based MRI contrast agents: Current status of clinical application. *Quantitative Imaging in Medicine and Surgery* **2011**, *1*, 35–40.

[47] Y.-X. J. Wang. Current status of superparamagnetic iron oxide contrast agents for liver magnetic resonance imaging. *World Journal of Gastroenterology* **2015**, *21*, 13400–13402.

[48] G. Liu, X. Song, K. W. Y. Chan, M. T. McMahon. Nuts and bolts of chemical exchange saturation transfer MRI. *NMR in Biomedicine* **2013**, *26*, 810–828.

[49] E. Terreno, D. D. Castelli, S. Aime. Encoding the frequency dependence in MRI contrast media: the emerging class of CEST agents. *Contrast Media & Molecular Imaging* **2010**, *5*, 78–98.

[50] A. D. Sherry, M. Woods. Chemical Exchange Saturation Transfer Contrast Agents for Magnetic Resonance Imaging. *Annual Review of Biomedical Engineering* **2008**, *10*, 391–411.

[51] E. B. Adamson, K. D. Ludwig, D. G. Mummy, S. B. Fain. Magnetic resonance imaging with hyperpolarized agents: methods and applications. *Physics in Medicine and Biology* **2017**, *62*, R81–R123.

[52] S. Månsson, E. Johansson, P. Magnusson, C.-M. Chai, G. Hansson, J. S. Petersson, F. Ståhlberg, K. Golman. 13C imaging—a new diagnostic platform. *European Radiology* **2005**, *16*, 57–67.

[53] S. B. Fain, F. R. Korosec, J. H. Holmes, R. O'Halloran, R. L. Sorkness, T. M. Grist. Functional lung imaging using hyperpolarized gas MRI. *Journal of Magnetic Resonance Imaging* **2007**, *25*, 910–923.

[54] A. Viale, F. Reineri, D. Santelia, E. Cerutti, S. Ellena, R. Gobetto, S. Aime. Hyperpolarized agents for advanced MRI investigations. *The Quarterly Journal of Nuclear Medicine and Molecular Imaging* **2009**, *53*, 604–617.

[55] A. E. J. de Nooy, A. C. Besemer, H. van Bekkum. On the Use of Stable Organic Nitroxyl Radicals for the Oxidation of Primary and Secondary Alcohols. *Synthesis* **1996**, *1996*, 1153–1176.

[56] K. Sato, T. Ono, Y. Sasano, F. Sato, M. Kumano, K. Yoshida, T. Dairaku, Y. Iwabuchi, Y. Kashiwagi. Electrochemical Oxidation of Amines Using a Nitroxyl Radical Catalyst and the Electroanalysis of Lidocaine. *Catalysts* **2018**, *8*, 649.

[57] A. Studer, T. Vogler. Applications of TEMPO in Synthesis. *Synthesis* **2008**, *2008*, 1979–1993.

[58] L. Tebben, A. Studer. Nitroxides: Applications in Synthesis and in Polymer Chemistry. *Angewandte Chemie International Edition* **2011**, *50*, 5034–5068.

[59] M. Shibuya, S. Nagasawa, Y. Osada, Y. Iwabuchi. Mechanistic Insight into Aerobic Alcohol Oxidation Using NO_x–Nitroxide Catalysis Based on Catalyst Structure–Activity Relationships. *The Journal of Organic Chemistry* **2014**, *79*, 10256–10268.

[60] J. Nicolas, Y. Guillaneuf, C. Lefay, D. Bertin, D. Gigmes, B. Charleux. Nitroxide-mediated polymerization. *Progress in Polymer Science* **2013**, *38*, 63–235.

[61] M. M. Haugland, J. E. Lovett, E. A. Anderson. Advances in the synthesis of nitroxide radicals for use in biomolecule spin labelling. *Chemical Society Reviews* **2018**, *47*, 668–680.

[62] S. Nakatsuji, H. Anzai. Recent progress in the development of organomagnetic materials based on neutral nitroxide radicals and charge transfer complexes derived from nitroxide radicals. *Journal of Materials Chemistry* **1997**, *7*, 2161–2174.

[63] S. J. Blundell, F. L. Pratt. Organic and molecular magnets. *Journal of Physics: Condensed Matter* **2004**, *16*, R771–R828.

[64] H. Nishide, K. Oyaizu. Toward Flexible Batteries. *Science* **2008**, *319*, 737–738.

[65] T. Janoschka, M. D. Hager, U. S. Schubert. Powering up the Future: Radical Polymers for Battery Applications. *Advanced Materials* **2012**, *24*, 6397–6409.

[66] E. P. Tomlinson, M. E. Hay, B. W. Boudouris. Radical Polymers and Their Application to Organic Electronic Devices. *Macromolecules* **2014**, *47*, 6145–6158.

[67] L. Wylie, K. Oyaizu, A. Karton, M. Yoshizawa-Fujita, E. I. Izgorodina. Toward Improved Performance of All-Organic Nitroxide Radical Batteries with Ionic Liquids: A Theoretical Perspective. *ACS Sustainable Chemistry & Engineering* **2019**, *7*, 5367–5375.

[68] Y. Xie, K. Zhang, M. J. Monteiro, Z. Jia. Conjugated Nitroxide Radical Polymers: Synthesis and Application in Flexible Energy Storage Devices. *ACS Applied Materials & Interfaces* **2019**, *11*, 7096–7103.

[69] R. C. Brasch. Work in progress: methods of contrast enhancement for NMR imaging and potential applications. A subject review. *Radiology* **1983**, *147*, 781–788.

[70] R. C. Brasch, D. A. London, G. E. Wesbey, T. N. Tozer, D. E. Nitecki, R. D. Williams, J. Doemeny, L. D. Tuck, D. P. Lallemand. Work in progress: nuclear magnetic resonance study of a paramagnetic nitroxide contrast agent for enhancement of renal structures in experimental animals. *Radiology* **1983**, *147*, 773–779.

[71] R. Brasch, D. Nitecki, M. Brant-Zawadzki, D. Enzmann, G. Wesbey, T. Tozer, L. Tuck, C. Cann, Fike, P. Sheldon. Brain nuclear magnetic resonance imaging enhanced by a paramagnetic nitroxide contrast agent: preliminary report. *American Journal of Roentgenology* **1983**, *141*, 1019–1023.

[72] V. Afzal, R. C. Brasch, D. E. Nitecki, S. Wolff. Nitroxyl Spin Label Contrast Enhancers for Magnetic Resonance Imaging: Studies of Acute Toxicity and Mutagenesis. *Investigative Radiology* **1984**, *19*, 549–552.

[73] R. L. Ehman, G. E. Wesbey, K. L. Moon, R. D. Williams, M. T. McNamara, W. R. Couet, T. N. Tozer, R. C. Brasch. Enhanced MRI of tumors utilizing a new nitroxyl spin label contrast agent. *Magnetic Resonance Imaging* **1985**, *3*, 89–97.

[74] W. R. Couet, U. G. Eriksson, T. N. Tozer, L. D. Tuck, G. E. Wesbey, D. Nitecki, R. C. Brasch. Pharmacokinetics and Metabolic Fate of Two Nitroxides Potentially Useful as Contrast Agents for Magnetic Resonance Imaging. *Pharmaceutical Research* **1984**, *01*, 203–209.

[75] K. Adamic, D. F. Bowman, K. U. Ingold. Self-reaction of diethylnitroxide radicals. *Journal of the American Chemical Society* **1970**, *92*, 1093–1094.

[76] A. Nilsen, R. Braslau. Nitroxide decomposition: Implications toward nitroxide design for applications in living free-radical polymerization.

Journal of Polymer Science Part A: Polymer Chemistry **2005**, *44*, 697–717.

[77] M. Amar, S. Bar, M. A. Iron, H. Toledo, B. Tumanskii, L. J. Shimon, M. Botoshansky, N. Fridman, A. M. Szpilman. Design concept for α-hydrogen-substituted nitroxides. *Nature Communications* **2015**, *6*, 6070.

[78] E. G. Rozantsev, V. D. Sholle. Synthesis and Reactions of Stable Nitroxyl Radicals II. Reactions. *Synthesis* **1971**, *1971*, 401–414.

[79] F. Hyodo, K. ichiro Matsumoto, A. Matsumoto, J. B. Mitchell, M. C. Krishna. Probing the Intracellular Redox Status of Tumors with Magnetic Resonance Imaging and Redox-Sensitive Contrast Agents. *Cancer Research* **2006**, *66*, 9921–9928.

[80] Z. Zhelev, R. Bakalova, I. Aoki, V. Gadjeva, I. Kanno. Imaging of cancer by redox-mediated mechanism: a radical diagnostic approach. *Molecular BioSystems* **2010**, *6*, 2386–2388.

[81] J. F. W. Keana, S. Pou, G. M. Rosen. Nitroxides as potential contrast enhancing agents for MRI application: Influence of structure on the rate of reduction by rat hepatocytes, whole liver homogenate, subcellular fractions, and ascorbate. *Magnetic Resonance in Medicine* **1987**, *5*, 525–536.

[82] J. P. Blinco, J. L. Hodgson, B. J. Morrow, J. R. Walker, G. D. Will, M. L. Coote, S. E. Bottle. Experimental and Theoretical Studies of the Redox Potentials of Cyclic Nitroxides. *The Journal of Organic Chemistry* **2008**, *73*, 6763–6771.

[83] Y. Kinoshita, K. ichi Yamada, T. Yamasaki, H. Sadasue, K. Sakai, H. Utsumi. Development of novel nitroxyl radicals for controlling reactivity with ascorbic acid. *Free Radical Research* **2009**, *43*, 565–571.

[84] J. T. Paletta, M. Pink, B. Foley, S. Rajca, A. Rajca. Synthesis and Reduction Kinetics of Sterically Shielded Pyrrolidine Nitroxides. *Organic Letters* **2012**, *14*, 5322–5325.

[85] T. Yamasaki, F. Mito, Y. Ito, S. Pandian, Y. Kinoshita, K. Nakano, R. Murugesan, K. Sakai, H. Utsumi, K. ichi Yamada. Structure-Reactivity Relationship of Piperidine Nitroxide: Electrochemical, ESR and Computational Studies. *The Journal of Organic Chemistry* **2011**, *76*, 435–440.

[86] S. Morris, G. Sosnovsky, B. Hui, C. Huber, N. Rao, H. Swartz. Chemical and Electrochemical Reduction Rates of Cyclic Nitroxides (Nitroxyls). *Journal of Pharmaceutical Sciences* **1991**, *80*, 149–152.

[87] S. Pou, P. L. Davis, G. L. Wolf, G. M. Rosen. Use of Nitroxides as NMR Contrast Enhancing Agents for Joints. *Free Radical Research* **1995**, *23*, 353–364.

[88] G. Bacic, K. J. Liu, F. Goda, P. J. Hoopes, G. M. Rosen, H. M. Swartz. MRI contrast enhanced study of cartilage proteoglycan degradation in the rabbit knee. *Magnetic Resonance in Medicine* **1997**, *37*, 764–768.

[89] V. I. Ovcharenko, E. Y. Fursova, T. G. Tolstikova, K. N. Sorokina, A. Y. Letyagin, A. A. Savelov. Imidazol-4-yl 2-Imidazoline Nitroxide Radicals, a New Class of Promising Contrast Agents for Magnetic Resonance Imaging. *Doklady Chemistry* **2005**, *404*, 171–173.

[90] A. A. Savelov, D. A. Kokorin, E. Y. Fursova, V. I. Ovcharenko. A stable nitroxide radical as a contrast agent for magnetic resonance imaging. *Doklady Chemistry* **2007**, *416*, 241–243.

[91] M. C. Emoto, K. ichi Yamada, M. Yamato, H. G. Fujii. Novel ascorbic acid-resistive nitroxide in a lipid emulsion: An efficient brain imaging contrast agent for MRI of small rodents. *Neuroscience Letters* **2013**, *546*, 11–15.

[92] W. M. Pardridge. Drug Transport across the Blood–Brain Barrier. *Journal of Cerebral Blood Flow & Metabolism* **2012**, *32*, 1959–1972.

[93] Z. Zhelev, R. Bakalova, I. Aoki, K. ichiro Matsumoto, V. Gadjeva, K. Anzai, I. Kanno. Nitroxyl radicals as low toxic spin-labels for non-invasive magnetic resonance imaging of blood–brain barrier permeability for conventional therapeutics. *Chem. Commun.* **2009**, 53–55.

[94] Z. Zhelev, R. Bakalova, I. Aoki, K. ichiro Matsumoto, V. Gadjeva, K. Anzai, I. Kanno. Nitroxyl Radicals for Labeling of Conventional Therapeutics and Noninvasive Magnetic Resonance Imaging of Their Permeability for Blood-Brain Barrier: Relationship between Structure, Blood Clearance, and MRI Signal Dynamic in the Brain. *Molecular Pharmaceutics* **2009**, *6*, 504–512.

[95] Z. Zhelev, V. Gadjeva, I. Aoki, R. Bakalova, T. Saga. Cell-penetrating nitroxides as molecular sensors for imaging of cancer *in vivo*, based on tissue redox activity. *Molecular BioSystems* **2012**, *8*, 2733–2740.

[96] M. C. Emoto, S. Sato, H. G. Fujii. Development of nitroxide-based theranostic compounds that act both as anti-inflammatory drugs and brain redox imaging probes in MRI. *Magnetic Resonance in Chemistry* **2016**, *54*, 705–711.

[97] Z. Zhelev, R. Bakalova, I. Aoki, D. Lazarova, T. Saga. Imaging of Superoxide Generation in the Dopaminergic Area of the Brain in Parkinson's Disease, Using Mito-TEMPO. *ACS Chemical Neuroscience* **2013**, *4*, 1439–1445.

[98] R. Bakalova, E. Georgieva, D. Ivanova, Z. Zhelev, I. Aoki, T. Saga. Magnetic Resonance Imaging of Mitochondrial Dysfunction and Metabolic Activity, Accompanied by Overproduction of Superoxide. *ACS Chemical Neuroscience* **2015**, *6*, 1922–1929.

[99] E. Tanimoto, S. Karasawa, S. Ueki, N. Nitta, I. Aoki, N. Koga. Unexpectedly large water-proton relaxivity of TEMPO incorporated into micelle-oligonucleotides. *RSC Advances* **2013**, *3*, 3531–3534.

[100] Y. Sato, H. Hayashi, M. Okazaki, M. Aso, S. Karasawa, S. Ueki, H. Suemune, N. Koga. Water-proton relaxivities of DNA oligomers carrying TEMPO radicals. *Magnetic Resonance in Chemistry* **2008**, *46*, 1055–1058.

[101] M. Okazaki, Y. Sato, S. Karasawa, N. Koga. Synthesis and Relaxivities of Oligonucleotides with TEMPO-labeled Sugar Moiety. *Nucleic Acids Symposium Series* **2008**, *52*, 375–376.

[102] M. Dharmarwardana, A. F. Martins, Z. Chen, P. M. Palacios, C. M. Nowak, R. P. Welch, S. Li, M. A. Luzuriaga, L. Bleris, B. S. Pierce, A. D. Sherry, J. J. Gassensmith. Nitroxyl Modified Tobacco Mosaic Virus as a Metal-Free High-Relaxivity MRI and EPR Active Superoxide Sensor. *Molecular Pharmaceutics* **2018**, *15*, 2973–2983.

[103] E. J. Rivera, R. Sethi, F. Qu, R. Krishnamurthy, R. Muthupillai, M. Alford, M. A. Swanson, S. S. Eaton, G. R. Eaton, L. J. Wilson. Nitroxide Radicals@US-Tubes: New Spin Labels for Biomedical Applications. *Advanced Functional Materials* **2012**, *22*, 3691–3698.

[104] K. Morishita, S. Murayama, T. Araki, I. Aoki, S. Karasawa. Thermal- and pH-Dependent Size Variable Radical Nanoparticles and Its Water Proton Relaxivity for Metal-Free MRI Functional Contrast Agents. *The Journal of Organic Chemistry* **2016**, *81*, 8351–8362.

[105] K. Morishita, Y. Okamoto, S. Murayama, K. Usui, E. Ohashi, G. Hirai, I. Aoki, S. Karasawa. Water-Proton Relaxivities of Radical Nanoparticles Self-Assembled via Hydration or Dehydration Processes. *Langmuir* **2017**, *33*, 7810–7817.

[106] J. M. W. Chan, R. J. Wojtecki, H. Sardon, A. L. Z. Lee, C. E. Smith, A. Shkumatov, S. Gao, H. Kong, Y. Y. Yang, J. L. Hedrick. Self-Assembled, Biodegradable Magnetic Resonance Imaging Agents: Organic Radical-Functionalized Diblock Copolymers. *ACS Macro Letters* **2017**, *6*, 176–180.

[107] K. Morishita, S. Ueki, Y. Fuchi, S. Murayama, T. Kaneko, N. Narita, S. Kobayashi, G. Hirai, I. Aoki, S. Karasawa. Self-Assembled Biradical Ureabenzene Nanoparticles for Magnetic Resonance Imaging. *ACS Applied Nano Materials* **2018**, *1*, 6967–6975.

[108] B. W. Muir, D. P. Acharya, D. F. Kennedy, X. Mulet, R. A. Evans, S. M. Pereira, K. L. Wark, B. J. Boyd, T.-H. Nguyen, T. M. Hinton, L. J. Waddington, N. Kirby, D. K. Wright, H. X. Wang, G. F. Egan, B. A. Moffat. Metal-free and MRI visible theranostic lyotropic liquid crystal nitroxide-based nanoparticles. *Biomaterials* **2012**, *33*, 2723–2733.

[109] L. Huang, C. Yan, D. Cui, Y. Yan, X. Liu, X. Lu, X. Tan, X. Lu, J. Xu, Y. Xu, R. Liu. Organic Radical Contrast Agents Based on Polyacetylenes Containing 2,2,6,6-Tetramethylpiperidine 1-Oxyl (TEMPO): Targeted Magnetic Resonance (MR)/Optical Bimodal Imaging of Folate Receptor Expressing HeLa Tumors in Vitro and in Vivoa. *Macromolecular Bioscience* **2015**, *15*, 788–798.

[110] X. Lu, Z. Zhang, Q. Xia, M. Hou, C. Yan, Z. Chen, Y. Xu, R. Liu. Glucose functionalized carbon quantum dot containing organic radical for optical/MR dual-modality bioimaging. *Materials Science and Engineering: C* **2018**, *82*, 190–196.

[111] C. S. Winalski, S. Shortkroff, R. V. Mulkern, E. Schneider, G. M. Rosen. Magnetic resonance relaxivity of dendrimer-linked nitroxides. *Magnetic Resonance in Medicine* **2002**, *48*, 965–972.

[112] A. J. Maliakal, N. J. Turro, A. W. Bosman, J. Cornel, E. W. Meijer. Relaxivity Studies on Dinitroxide and Polynitroxyl Functionalized Dendrimers: Effect of Electron Exchange and Structure on Paramagnetic Relaxation Enhancement. *The Journal of Physical Chemistry A* **2003**, *107*, 8467–8475.

[113] G. Francese, F. A. Dunand, C. Loosli, A. E. Merbach, S. Decurtins. Functionalization of PAMAM dendrimers with nitronyl nitroxide radicals as models for the outer-sphere relaxation in dentritic potential MRI contrast agents. *Magnetic Resonance in Chemistry* **2003**, *41*, 81–83.

[114] M. Gussoni, F. Greco, P. Ferruti, E. Ranucci, A. Ponti, L. Zetta. Poly(amidoamine)s carrying TEMPO residues for NMR imaging applications. *New J. Chem.* **2008**, *32*, 323–332.

[115] A. Rajca, Y. Wang, M. Boska, J. T. Paletta, A. Olankitwanit, M. A. Swanson, D. G. Mitchell, S. S. Eaton, G. R. Eaton, S. Rajca. Organic Radical Contrast Agents for Magnetic Resonance Imaging. *Journal of the American Chemical Society* **2012**, *134*, 15724–15727.

[116] H. Sato, V. Kathirvelu, G. Spagnol, S. Rajca, A. Rajca, S. S. Eaton, G. R. Eaton. Impact of Electron-Electron Spin Interaction on Electron Spin Relaxation of Nitroxide Diradicals and Tetraradical in Glassy Solvents Between 10 and 300 K. *The Journal of Physical Chemistry B* **2008**, *112*, 2818–2828.

[117] A. Olankitwanit, V. Kathirvelu, S. Rajca, G. R. Eaton, S. S. Eaton, A. Rajca. Calix[4]arene nitroxide tetraradical and octaradical. *Chemical Communications* **2011**, *47*, 6443–6445.

[118] A. Rajca, S. Mukherjee, M. Pink, S. Rajca. Exchange Coupling Mediated Through-Bonds and Through-Space in Conformationally Constrained Polyradical Scaffolds: Calix[4]arene Nitroxide Tetraradicals and Diradical. *Journal of the American Chemical Society* **2006**, *128*, 13497–13507.

[119] Y. Huang, A. Nan, G. M. Rosen, C. S. Winalski, E. Schneider, P. Tsai, H. Ghandehari. *N*-(2-Hydroxypropyl)methacrylamide(HPMA) Copolymer-Linked Nitroxides: Potential Magnetic Resonance Contrast Agents. *Macromolecular Bioscience* **2003**, *3*, 647–652.

[120] H. V.-T. Nguyen, Q. Chen, J. T. Paletta, P. Harvey, Y. Jiang, H. Zhang, M. D. Boska, M. F. Ottaviani, A. Jasanoff, A. Rajca, J. A. Johnson. Nitroxide-Based Macromolecular Contrast Agents with Unprecedented Transverse Relaxivity and Stability for Magnetic Resonance Imaging of Tumors. *ACS Central Science* **2017**, *3*, 800–811.

[121] H. V.-T. Nguyen, A. Detappe, N. M. Gallagher, H. Zhang, P. Harvey, C. Yan, C. Mathieu, M. R. Golder, Y. Jiang, M. F. Ottaviani, A. Jasanoff, A. Rajca, I. Ghobrial, P. P. Ghoroghchian, J. A. Johnson. Triply Loaded Nitroxide Brush-Arm Star Polymers Enable Metal-Free Millimetric Tumor Detection by Magnetic Resonance Imaging. *ACS Nano* **2018**, *12*, 11343–11354.

[122] G. G. Alvaradejo, H. V.-T. Nguyen, P. Harvey, N. M. Gallagher, D. Le, M. F. Ottaviani, A. Jasanoff, G. Delaittre, J. A. Johnson. Polyoxazoline-

Based Bottlebrush and Brush-Arm Star Polymers via ROMP: Syntheses and Applications as Organic Radical Contrast Agents. *ACS Macro Letters* **2019**, *8*, 473–478.

[123] A. L. Kleschyov, V. Sen', V. Golubev, K. Münnemann, D. Hinderberger, K. J. Lackner, S. Weber, M. Terekhov, L. M. Schreiber, T. Münzel. Heparin–polynitroxides: Synthesis and preliminary evaluation as cardiovascular EPR/MR imaging probes and extracellular space-targeted antioxidants. *European Journal of Medicinal Chemistry* **2012**, *58*, 265–271.

[124] S. Garmendia, D. Mantione, S. A. de Castro, C. Jehanno, L. Lezama, J. L. Hedrick, D. Mecerreyes, L. Salassa, H. Sardon. Polyurethane based organic macromolecular contrast agents (PU-ORCAs) for magnetic resonance imaging. *Polymer Chemistry* **2017**, *8*, 2693–2701.

[125] H. Hayashi, S. Karasawa, A. Tanaka, K. Odoi, K. Chikama, H. Kuribayashi, N. Koga. Water-proton relaxivity of hyperbranched polymers carrying TEMPO radicals. *Magnetic Resonance in Chemistry* **2009**, *47*, 201–204.

[126] W. L. Hubbell, D. S. Cafiso, C. Altenbach. Identifying conformational changes with site-directed spin labeling. *Nature Structural Biology* **2000**, *7*, 735–739.

[127] V. Khramtsov, L. Weiner, I. Grigoriev, L. Volodarsky. Proton exchange in stable nitroxyl radicals. EPR study of the pH of aqueous solutions. *Chemical Physics Letters* **1982**, *91*, 69–72.

[128] I. A. Kirilyuk, A. A. Bobko, I. A. Grigorev, V. V. Khramtsov. Synthesis of the tetraethyl substituted pH-sensitive nitroxides of imidazole series with enhanced stability towards reduction. *Organic & Biomolecular Chemistry* **2004**, *2*, 1025–1030.

[129] H. M. Swartz, K. Chen, M. Pals, M. Sentjurc, P. D. Morse. Hypoxia-sensitive NMR contrast agents. *Magnetic Resonance in Medicine* **1986**, *3*, 169–174.

[130] H. M. Swartz. Use of nitroxides to measure redox metabolism in cells and tissues. *Journal of the Chemical Society, Faraday Transactions 1: Physical Chemistry in Condensed Phases* **1987**, *83*, 191–202.

[131] Y. Y. Woldman, S. V. Semenov, A. A. Bobko, I. A. Kirilyuk, J. F. Polienko, M. A. Voinov, E. G. Bagryanskaya, V. V. Khramtsov. Design of liposome-based pH sensitive nanoSPIN probes: nano-sized particles with incorporated nitroxides. *The Analyst* **2009**, *134*, 904–910.

[132] S. Kempe, H. Metz, K. Mäder. Application of Electron Paramagnetic Resonance (EPR) spectroscopy and imaging in drug delivery research – Chances and challenges. *European Journal of Pharmaceutics and Biopharmaceutics* **2010**, *74*, 55–66.

[133] S. Posse, R. Otazo, S. R. Dager, J. Alger. MR spectroscopic imaging: Principles and recent advances. *Journal of Magnetic Resonance Imaging* **2012**, *37*, 1301–1325.

[134] M. H. Buonocore, R. J. Maddock. Magnetic resonance spectroscopy of the brain: a review of physical principles and technical methods. *Reviews in the Neurosciences* **2015**, *26*, 609–632.

[135] E. G. W. ter Voert, L. Heijmen, H. W. M. van Laarhoven, A. Heerschap. *In vivo* magnetic resonance spectroscopy of liver tumors and metastases. *World Journal of Gastroenterology* **2011**, *17*, 5133–5149.

[136] J. Kurhanewicz, M. G. Swanson, S. J. Nelson, D. B. Vigneron. Combined magnetic resonance imaging and spectroscopic imaging approach to molecular imaging of prostate cancer. *Journal of Magnetic Resonance Imaging* **2002**, *16*, 451–463.

[137] D. Bertholdo, A. Watcharakorn, M. Castillo. Brain Proton Magnetic Resonance Spectroscopy. *Neuroimaging Clinics of North America* **2013**, *23*, 359–380.

[138] M. Malet-Martino, U. Holzgrabe. NMR techniques in biomedical and pharmaceutical analysis. *Journal of Pharmaceutical and Biomedical Analysis* **2011**, *55*, 1–15.

[139] J. R. Alger. Quantitative Proton Magnetic Resonance Spectroscopy and Spectroscopic Imaging of the Brain. *Topics in Magnetic Resonance Imaging* **2010**, *21*, 115–128.

[140] A. Haase, J. Frahm, W. Hanicke, D. Matthaei. ^{1}H NMR chemical shift selective (CHESS) imaging. *Physics in Medicine and Biology* **1985**, *30*, 341–344.

[141] R. Ogg, R. Kingsley, J. Taylor. WET, a T_1- and B_1-Insensitive Water-Suppression Method for in Vivo Localized ^{1}H NMR Spectroscopy. *Journal of Magnetic Resonance, Series B* **1994**, *104*, 1–10.

[142] I. Tkac, Z. Starcuk, I.-Y. Choi, R. Gruetter. In vivo ^{1}H NMR spectroscopy of rat brain at 1 ms echo time. *Magnetic Resonance in Medicine* **1999**, *41*, 649–656.

[143] P. A. Bottomley. Spatial Localization in NMR Spectroscopy *in vivo*. *Annals of the New York Academy of Sciences* **1987**, *508*, 333–348.

[144] J. Frahm, K.-D. Merboldt, W. Hänicke. Localized proton spectroscopy using stimulated echoes. *Journal of Magnetic Resonance (1969)* **1987**, *72*, 502–508.

[145] W. Willker, D. Leibfritz, R. Kerssebaum, W. Bermel. Gradient selection in inverse heteronuclear correlation spectroscopy. *Magnetic Resonance in Chemistry* **1993**, *31*, 287–292.

[146] S. Liu. The role of coordination chemistry in the development of target-specific radiopharmaceuticals. *Chemical Society Reviews* **2004**, *33*, 445–461.

[147] M. G. V. Heiden, L. C. Cantley, C. B. Thompson. Understanding the Warburg Effect: The Metabolic Requirements of Cell Proliferation. *Science* **2009**, *324*, 1029–1033.

[148] H. N. Christensen. Role of amino acid transport and countertransport in nutrition and metabolism. *Physiological Reviews* **1990**, *70*, 43–77.

[149] J. W. Fletcher, B. Djulbegovic, H. P. Soares, B. A. Siegel, V. J. Lowe, G. H. Lyman, R. E. Coleman, R. Wahl, J. C. Paschold, N. Avril, L. H. Einhorn, W. W. Suh, D. Samson, D. Delbeke, M. Gorman, A. F. Shields. Recommendations on the Use of ^{18}F-FDG PET in Oncology. *Journal of Nuclear Medicine* **2008**, *49*, 480–508.

[150] A. W. J. M. Glaudemans, R. H. Enting, M. A. A. M. Heesters, R. A. J. O. Dierckx, R. W. J. van Rheenen, A. M. E. Walenkamp, R. H. J. A. Slart. Value of ^{11}C-methionine PET in imaging brain tumours and metastases. *European Journal of Nuclear Medicine and Molecular Imaging* **2012**, *40*, 615–635.

[151] T. Schulte, K. O. Siegenthaler, H. Luftmann, M. Letzel, A. Studer. Nitroxide-Mediated Polymerization N-Isopropylacrylamide: Electrospray Ionization Mass Spectrometry, Matrix-Assisted Laser Desorption Ionization Mass Spectrometry, and Multiple-Angle Laser Light Scattering Studies on Nitroxide-Terminated Poly-N-isopropylacrylamides. *Macromolecules* **2005**, *38*, 6833–6840.

[152] K. Sakai, K. ichi Yamada, T. Yamasaki, Y. Kinoshita, F. Mito, H. Utsumi. Effective 2,6-substitution of piperidine nitroxyl radical by carbonyl compound. *Tetrahedron* **2010**, *66*, 2311–2315.

[153] X. Wang, M. Emoto, A. Sugimoto, Y. Miyake, K. Itto, M. Amasaka, S. Xu, H. Hirata, H. Fujii, H. Arimoto. Synthesis of ^{15}N-labeled 4-oxo-2,2,6,6-tetraethylpiperidine nitroxide for EPR brain imaging. *Tetrahedron Letters* **2014**, *55*, 2146–2149.

[154] S. Sato, T. Kumazawa, S. Matsuba, J. ichi Onodera, M. Aoyama, H. Obara, H. Kamada. Novel glycosylation of the nitroxyl radicals with peracetylated glycosyl fluorides using a combination of $BF_3{\cdot}OEt_2$ and an amine base as promoters. *Carbohydrate Research* **2001**, *334*, 215–222.

[155] K. ichi Yamada, Y. Kinoshita, T. Yamasaki, H. Sadasue, F. Mito, M. Nagai, S. Matsumoto, M. Aso, H. Suemune, K. Sakai, H. Utsumi. Synthesis of Nitroxyl Radicals for Overhauser-enhanced Magnetic Resonance Imaging. *Archiv der Pharmazie* **2008**, *341*, 548–553.

[156] A. Steinmann, J. Thimm, M. Matwiejuk, J. Thiem. Formation of Homooligosaccharides Using Base-Promoted Glycosylation of Unprotected Glycosyl Fluorides. *Macromolecules* **2010**, *43*, 3606–3612.

[157] M. Becker, L. D. Cola, A. Studer. Assembly of linear chains consisting of alternating silica beads and zeolite L crystals by nitroxide exchange reactions. *Journal of Materials Chemistry C* **2013**, *1*, 3287–3290.

[158] B. Liu, C. Cui, W. Duan, M. Zhao, S. Peng, L. Wang, H. Liu, G. Cui. Synthesis and evaluation of anti-tumor activities of N^4 fatty acyl amino acid derivatives of 1-β-arabinofuranosylcytosine. *European Journal of Medicinal Chemistry* **2009**, *44*, 3596–3600.

[159] S. Sato, M. Yamaguchi, A. Nagai, R. Onuma, M. Saito, R. Sugawara, S. Shinohara, E. Okabe, T. Ito, T. Ogata. Evaluation of glucose-linked nitroxide radicals for use as an in vivo spin-label probe. *Spectrochimica Acta Part A: Molecular and Biomolecular Spectroscopy* **2014**, *124*, 322–327.

[160] O. Saphier, T. Silberstein, A. Shames, G. Likhtenshtein, E. Maimon, D. Mankuta, M. Mazor, M. Katz, D. Meyerstein, N. Meyerstein. The Reduction of a Nitroxide Spin Label as a Probe of Human Blood Antioxidant Properties. *Free Radical Research* **2003**, *37*, 301–308.

[161] J. Homer, M. S. Beevers. Driven-equilibrium single-pulse observation of T_1 relaxation. A reevaluation of a rapid "new" method for determining NMR spin-lattice relaxation times. *Journal of Magnetic Resonance (1969)* **1985**, *63*, 287–297.

[162] F. Hyodo, R. Murugesan, K. ichiro Matsumoto, E. Hyodo, S. Subramanian, J. B. Mitchell, M. C. Krishna. Monitoring redox-sensitive paramagnetic contrast agent by EPRI, OMRI and MRI. *Journal of Magnetic Resonance* **2008**, *190*, 105–112.

[163] K. ichiro Matsumoto, M. Narazaki, H. Ikehira, K. Anzai, N. Ikota. Comparisons of EPR imaging and T_1-weighted MRI for efficient imaging of nitroxyl contrast agents. *Journal of Magnetic Resonance* **2007**, *187*, 155–162.

[164] R. Autar, A. S. Khan, M. Schad, J. Hacker, R. M. J. Liskamp, R. J. Pieters. Adhesion Inhibition of F1C-Fimbriated Escherichia coli and Pseudomonas aeruginosa PAK and PAO by Multivalent Carbohydrate Ligands. *ChemBioChem* **2003**, *4*, 1317–1325.

[165] C. S. Rye, S. G. Withers. Glycosidase mechanisms. *Current Opinion in Chemical Biology* **2000**, *4*, 573–580.

Appendix

I. **M. Soikkeli**, K. Sievänen, J. Peltonen, T. Kaasalainen, M. Timonen, P. Heinonen, S. Rönkkö, V.-P. Lehto, J. Kavakka and S. Heikkinen. Synthesis and *in vitro* phantom NMR and MRI studies of fully organic free radicals, TEEPO-glucose and TEMPO-glucose, potential contrast agents for MRI. *RSC Adv.* **2015**, *5*, 15507 - 15510.

II. **M. Soikkeli**, K. Horkka, J.O. Moilanen, M. Timonen, J. Kavakka and S. Heikkinen. Synthesis, Stability and Relaxivity of TEEPO-Met: An Organic Radical as a Potential Tumor Targeting Contrast Agent for Magnetic Resonance Imaging. *Molecules* **2018**, *23*, 1034.

III. **M. Soikkeli**, M.I. Kettunen, R. Nivajärvi, V. Olsson, S. Rönkkö, J.P. Laakkonen, V.-P. Lehto, J. Kavakka and S. Heikkinen. Assessment of the Relaxation Enhancing Properties of a Nitroxide-Based Contrast Agent TEEPO-Glc with *in vivo* Magnetic Resonance Imaging. *Submitted*